ARTICLE

Tumor suppressor BAP1 nuclear import is governed by transportin-1

Tzu-Jing Yang[1,2] [iD], Tian-Neng Li[3], Rih-Sheng Huang[1] [iD], Max Yu-Chen Pan[3] [iD], Shu-Yu Lin[1,4] [iD], Steven Lin[1,2] [iD], Kuen-Phon Wu[1,2] [iD], Lily Hui-Ching Wang[3] [iD], and Shang-Te Danny Hsu[1,2] [iD]

Subcellular localization of the deubiquitinating enzyme BAP1 is deterministic for its tumor suppressor activity. While the monoubiquitination of BAP1 by an atypical E2/E3-conjugated enzyme UBE2O and BAP1 auto-deubiquitination are known to regulate its nuclear localization, the molecular mechanism by which BAP1 is imported into the nucleus has remained elusive. Here, we demonstrated that transportin-1 (TNPO1, also known as Karyopherin β2 or Kapβ2) targets an atypical C-terminal proline-tyrosine nuclear localization signal (PY-NLS) motif of BAP1 and serves as the primary nuclear transporter of BAP1 to achieve its nuclear import. TNPO1 binding dissociates dimeric BAP1 and sequesters the monoubiquitination sites flanking the PY-NLS of BAP1 to counteract the function of UBE2O that retains BAP1 in the cytosol. Our findings shed light on how TNPO1 regulates the nuclear import, self-association, and monoubiquitination of BAP1 pertinent to oncogenesis.

Introduction

BRCA1-associated protein 1 (BAP1) is a multidomain deubiquitinase (DUB) with a ubiquitin C-terminal hydrolase (UCH) domain at its N-terminus (Jensen et al., 1998). Unlike the other three human UCH paralogs (UCHL1, UCHL3, and UCHL5), BAP1 harbors two putative nuclear localization signals (NLSs) within its C-terminal domain (CTD) and is found predominantly inside the nucleus (Ventii et al., 2008; Jensen et al., 1998). BAP1 is an integral part of the polycomb repressive DUB complex or the BAP1-core complexes encompassing several transcription factors and/or chromatin remodeling factors, including HCF-1, ASXL1/2/3, FOXK1/2, YY1, and KLF5 (Sahtoe et al., 2016; Qin et al., 2015; Ji et al., 2014; Baymaz et al., 2014; Misaghi et al., 2009; Yu et al., 2010). The DUB activity of BAP1 is implicated in diverse cellular pathways, including cell proliferation (Machida et al., 2009; Qin et al., 2015), cell cycle progression (Pan et al., 2015; Eletr and Wilkinson, 2011), cell death (He et al., 2019; Sime et al., 2018), and DNA repair (Ventii et al., 2008; Misaghi et al., 2009; Nishikawa et al., 2009). A large number of mutations in BAP1 have been linked to human malignancies, including malignant mesothelioma, uveal melanoma, clear cell renal cell carcinoma, and cutaneous carcinoma. Loss of the DUB activity of BAP1 is considered to be the main contributing factor of BAP1-dependent malignancies (Ventii et al., 2008; Harbour et al., 2010; Testa et al., 2011; Carbone et al., 2013). In addition to

enzymatic dysfunction, cellular mislocalization of BAP1 is associated with multiple aggressive tumors. Loss of BAP1 within the nucleus was found in 50% of all uveal melanoma tissue specimens with increased risks of metastasis (Koopmans et al., 2014; Kalirai et al., 2014). A distinct focal perinuclear localization of BAP1 was found in 31% of all nuclear BAP1 negative uveal melanomas (Farquhar et al., 2018). In one study, 63% of malignant mesothelioma biopsy specimens exhibited loss of nuclear BAP1 (Carbone et al., 2016). Therefore, the absence of nuclear BAP1 is considered a prognostic hallmark for these aggressive cancers.

While BAP1 primarily functions as a transcription regulator, which requires its nuclear localization, Bononi et al. (2017) reported a novel function of cytoplasmic BAP1 that deubiquitinates and therefore stabilizes the type 3 inositol-1,4,5-trisphosphate receptor (IP_3R_3) at the mitochondria-associated ER membranes, thereby facilitating Ca^{2+}-mediated mitochondrial apoptosis. The lower levels of BAP1 in heterozygous $BAP1^{+/-}$ carriers led to the reduction of IP_3R_3 and hence deficient mitochondrial apoptosis that potentiates oncogenesis (Bononi et al., 2017). This finding underscores the biological relevance of subcellular localization of BAP1. The nuclear localization of BAP1 can be regulated by a ubiquitin-conjugating enzyme, UBE2O, that displays both E2 and E3 ubiquitin ligase activity. UBE2O multi-monoubiquitinates BAP1, thereby promoting the export of BAP1 from the nucleus

....

[1]Institute of Biological Chemistry, Academia Sinica, Taipei, Taiwan;   [2]Institute of Biochemical Sciences, National Taiwan University, Taipei, Taiwan;   [3]Institute of Molecular and Cellular Biology, National Tsing Hua University, Hsinchu, Taiwan;   [4]Academia Sinica Common Mass Spectrometry Facilities for Proteomics and Protein Modification Analysis, Academia Sinica, Taipei, Taiwan.

Correspondence to Shang-Te Danny Hsu: sthsu@gate.sinica.edu.tw.

to the cytosol (Mashtalir et al., 2014; Ullah et al., 2019; Klemperer et al., 1989; Berleth and Pickart, 1996). However, comprehensive understanding with regard to the mechanism by which the trafficking of BAP1 between the nucleus and cytoplasm is regulated remains lacking and warrants further studies.

In this study, we demonstrated that transportin-1 (TNPO1) mediates the nuclear import of BAP1 by recognizing an atypical NLS, namely proline-tyrosine (PY)-NLS, within the CTD of BAP1. TNPO1 exhibits a strong binding affinity toward the NLS of BAP1 to outcompete other nuclear import factors. Our biophysical findings were verified by CRISPR/Cas9-based knockout (KO) of the *TNPO1* gene that led to significantly increased cytoplasmic retention of BAP1, confirming that TNPO1 is the primary regulator of the nuclear import of BAP1. TNPO1 dissociates the CTD-mediated self-association of BAP to form a stoichiometric heterodimer. We further solved the crystal structure of TNPO1 in complex with the PY-NLS of BAP1 to demonstrate in conjunction with an in vitro monoubiquitination (mUb) assay that TNPO1 binding interferes with the UBE2O-mediated multi-mUb. Collectively, our findings established a versatile role of TNPO1 in regulating the nuclear import, oligomerization, and ubiquitination of BAP1.

Results

Identification of nuclear import factor of BAP1
BAP1 contains two distinct NLSs in its CTD, including a monopartite classical NLS (NLS1, [656]KRKKFK[661]) and a bipartite classic NLS (NLS2, [699]RRRQGVSIGRLHKQRKPDRRKRSR[722]). In addition, BAP1 harbors a nonclassical PY-NLS with both hydrophobic residue and basic residue-abundant epitopes ([703]GVSIGRLHKQRKPDRRKRSRPY[724]) that has a significant overlap with the sequences of NLS2 (Fig. 1 A).

To dissect the contributions of the individual NLSs in the context of nuclear import, we quantified the subcellular localizations of BAP1 in HeLa cells by live-cell imaging. In addition to WT BAP1 (hereafter BAP1$_{WT}$), we constructed a BAP1 variant harboring a nonsense mutation Q684* (hereafter BAP1$_{Q684*}$) that is prevalent in several cancers according to the COSMIC (https://cancer.sanger.ac.uk/cosmic) and cBioPortal (https://www.cbioportal.org) cancer databases. The C-terminal truncation caused by Q684* resulted in loss of the NLS2 while retaining the NLS1 (Fig. 1 A). A SNAP-tag was introduced to the N-termini of BAP1$_{WT}$ and BAP1$_{Q684*}$ for fluorescence imaging in live cells. Quantitation of the subcellular distributions of the BAP1 variants showed that BAP1$_{WT}$ predominately localized in the nucleus, whereas BAP1$_{Q684*}$ predominantly localized in the cytosol (Fig. 1, B and C), confirming an earlier observation that NLS2 is the essential NLS for nuclear import of BAP1 (Ventii et al., 2008).

To identify potential cellular factors pertinent to the nuclear import of BAP1, we transiently expressed an N-terminally FLAG-tagged BAP1 in HEK293 freestyle (HEK293F) cells as a bait to pull down BAP1-interacting proteins for mass spectrometry (MS)–based proteomic analysis (Fig. 1 D). We identified 1,149 BAP1-interacting proteins, including many well-established BAP1 interaction partners, namely HCF-1, *O*-GlcNAc transferase (OGT1), transcription factors Forkhead Box K1 and K2 (FOXK1

and FOXK2), and an atypical E2/E3 conjugated enzyme, UBE2O. In addition, we found VDAC1 and GRP75, which interact with IP$_3$R$_3$ to form a transient Ca^{2+}-controlling machinery that is a substrate of BAP1 (Bononi et al., 2017). Five 14-3-3 protein isoforms (14-3-3-β, γ, θ, -ε, and -ζ) that interact with BAP1 to induce cell death in neuroblastoma were also identified (Table S1; Sime et al., 2018).

To focus on proteins involved in the nuclear localization of BAP1, we chose those that fall into the categories of "regulation of protein import into the nucleus," "NLS-bearing protein import into nucleus," "import into nucleus," and "protein localization to nucleus" according to Gene Ontology analysis (Fig. 1 E and Table S1). We found five karyopherin-α paralogs, including importin α5 (KPNA1), α1 (KPNA2), α4 (KPNA3), α3 (KPNA4), and α7 (KPNA6), and seven karyopherin-β paralogs, including importin β1, importin-4 (IPO4), -5 (IPO5), -7 (IPO7), -9 (IPO9), TNPO1 (KPNB2, also known as Kapβ2), and transportin-2 (Fig. 1 E and Table S1). Importin-β generally requires importin-α as the adaptor for the initial protein cargo recognition to form the cargo:importin factors ternary complex (Pumroy and Cingolani, 2015). The importin-α/β system mediates the nuclear import of protein cargos that harbor classical NLSs (cNLSs). In contrast, transportins have an all-in-one function that engages both initial recognition and nuclear import of PY-NLS–containing cargos without the need for auxiliary adaptors (Lee et al., 2006; Twyffels et al., 2014). The cargo:nuclear import factor complexes subsequently pass through the nuclear pore complexes, traversing the nuclear envelope to the nucleus. Since BAP1 possesses recognition motifs for both the importin-α/β and transportins systems, the identification of multiple BAP1-associated nuclear import factors suggested some redundancy in the nuclear localization pathways for BAP1.

The nuclear import of BAP1 is primarily mediated by TNPO1
According to the exponentially modified protein abundance index (emPAI) of identified nuclear import factors from the proteomic results, we focused on three candidates with the highest emPAIs, namely TNPO1 (emPAI: 0.58), importin α5 (emPAI: 0.43), and importin α1 (emPAI: 0.34) to examine their physical interactions with BAP1 (Fig. 1 E). Recombinant importin-αs and TNPO1 were expressed in *Escherichia coli* and purified to homogeneity to investigate their interactions with the CTD of BAP1 (residues 596–729) fused with a maltose-binding protein (MBP) tag (hereafter MBP-BAP1$_{CTD}$) by size-exclusion chromatography (SEC; Fig. 2). In the presence of two-fold excess karyopherins, MBP-BAP1$_{CTD}$ formed stable complexes with individual karyopherins and coeluted at earlier elution volumes than did isolated proteins (Fig. 2 A). The formation of the binary complexes was confirmed by SDS-PAGE, which showed distinct protein bands of the early elution peaks, corresponding to MBP-BAP1$_{CTD}$ and individual karyopherins (Fig. 2 B).

To quantify the binding affinities of individual karyopherins to BAP1$_{CTD}$, we synthesized a FITC-labeled peptide corresponding to residues 699–729 of BAP1 (hereafter FITC-BAP1$_{699-729}$) for fluorescence polarization (FP) analysis to quantify the binding affinities of individual karyopherins to BAP1$_{CTD}$. Among the three karyopherins, TNPO1 exhibited the lowest dissociation
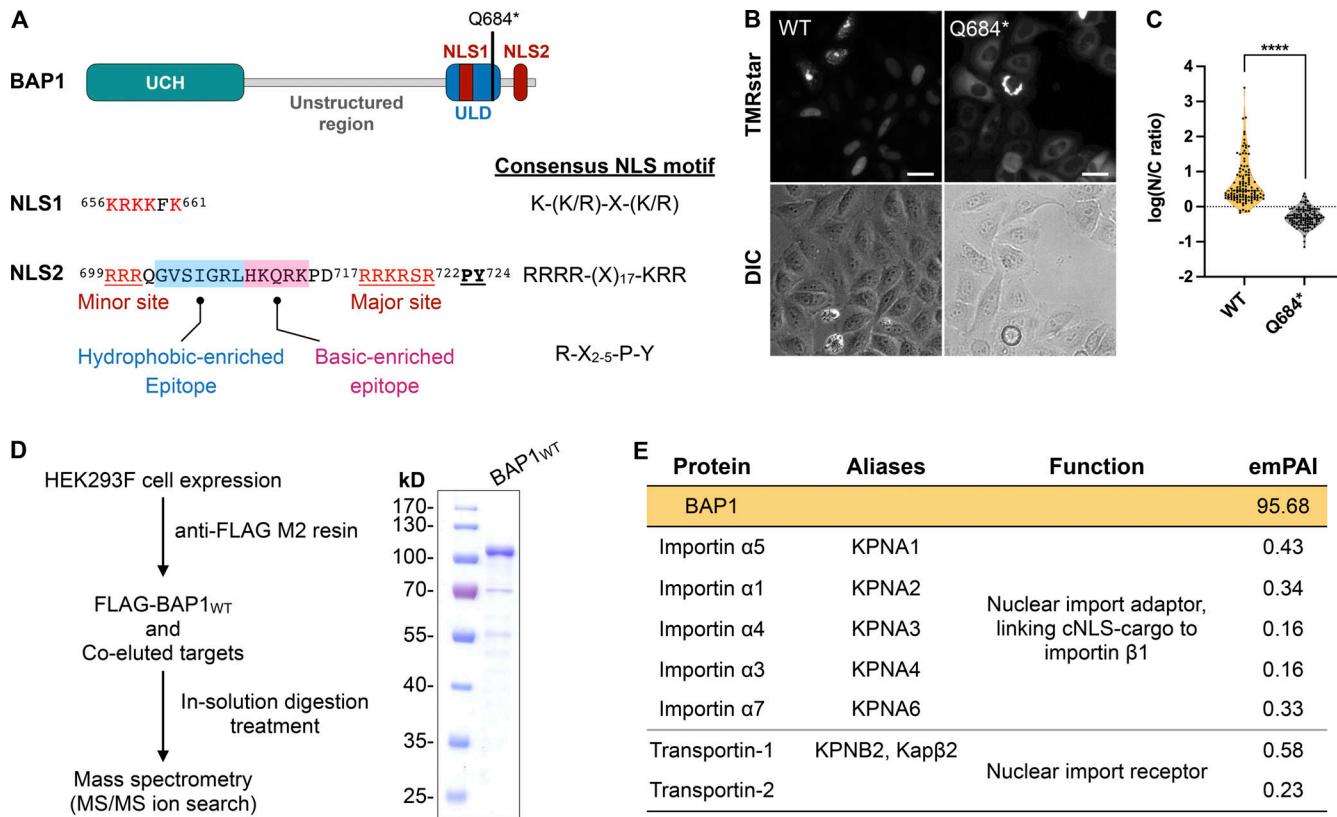
Figure 1. **Identification of motifs and cellular factors governing the nuclear import of BAP1. (A)** Domain structure and nuclear localization sequences of BAP1. BAP1 has two putative classic NLSs within the CTD of BAP1. NLS2 harbors a bipartite NLS and a PY-NLS. Two types of the N-terminal epitope of the PY-NLS motif, including hydrophobic and basic-enriched epitopes, are colored in light blue and light pink, respectively. **(B)** Live-cell imaging of BAP1 subcellular localization in HeLa cells expressing *BAP1 wild-type* (WT) and *BAP1_{Q684*}* (Q684*). SNAP-tagged BAP1 variants were probed by TMRstar. DIC, differential interference contrast imaging. Scale bars = 25 μm. **(C)** Nuclear-to-cytoplasmic ratio for the C-terminal deletion BAP1_{Q684*} compared with BAP1_{WT}. P value was calculated by unpaired, two-tailed *t* test; ****, P < 0.0001. Sample sizes (*n*) of SNAP-BAP1_{WT}- and SNAP-BAP1_{Q684*}–expressed cells: 119 and 118, respectively. **(D)** Workflow of BAP1-associated protein identification. Purified FLAG-BAP1_{WT} from affinity purification was verified by SDS-PAGE and stained with Coomassie blue. **(E)** Identification of nuclear import factors associated with BAP1 in the AP-MS analysis. Source data are available for this figure: SourceData F1.

constant (K_d) of 19.6 nM, whereas the K_d values of importin α5 and α1 were 0.67 μM and >7.2 μM, respectively, corresponding to a 34-fold and >360-fold increase compared with that of TNPO1 (Fig. 3). The results confirmed the physical interactions between BAP1 and the three karyopherins. The results also suggested that the NLS of BAP1 may be preferentially recognized by TNPO1 over importin α5 and α1 for nuclear import.

To validate our biophysical findings in cells, we individually knocked out the *TNPO1* (encoding TNPO1), *KPNA1* (importin α5), and *KPNA2* (importin α1) genes using CRISPR-Cas9 genome editing technology in HEK293 cells (Fig. S1). We performed immunofluorescence microscopy to assess the nuclear localization of endogenous BAP1 or ectopically expressed SNAP-BAP1 in these karyopherin-KO cells. Of the three KO cell lines, *TNPO1*-KO cells exhibited the most significant BAP1 retention in the cytosol (Fig. 4 A). A small portion of nuclear BAP1 signals in the *KPNA1*-KO cells was observed. In contrast, most BAP1 was found in the nuclei of the *KPNA2*-KO cells. Quantitation of the nucleus/cytoplasm fraction of BAP1 indicated the least amount of nuclear BAP1 in *TNPO1*-KO cells (0.21), compared with *KPNA1*-KO cells (0.44) and *KPNA2*-KO cells (0.64; Fig. 4 B). These findings confirmed our hypothesis of the dominant role of TNPO1 in BAP1

nuclear localization, while importin α5 and α1 may provide functional redundancy to TNPO1.

TNPO1 regulates CTD-mediated self-association of BAP1

To evaluate the binding stoichiometry between TNPO1 and BAP1, we used SEC coupled with multiangle light scattering (MALS). MBP-BAP1_{CTD} by itself displayed protein concentration–dependent oligomerization with an apparent mol wt of 92.0–109.8 kD on increasing protein concentration ≤60 μM (Fig. 5 A). As the theoretical mol wt of an MBP-BAP1_{CTD} monomer is 59 kD, the results suggested a dynamic monomer-dimer equilibrium for MBP-BAP1_{CTD}. Indeed, the C-terminal UCH37-like domain (ULD)-mediated dimerization is found in a BAP1 ortholog from *Drosophila melanogaster*, Calypso (Foglizzo et al., 2018). The NLS motif of Calypso is located beyond residue 430, and AlphaFold cannot confidently model its structure (Jumper et al., 2021; Varadi et al., 2022). Likewise, the two NLS motifs of BAP1 are connected to the ULD through a very long disordered loop, and their structures and relative positions with respect to the remaining folded structure cannot be reliably predicted by AlphaFold. While structural information of BAP1 is currently lacking, BAP1 and Calypso share the same coiled-coil ULD that
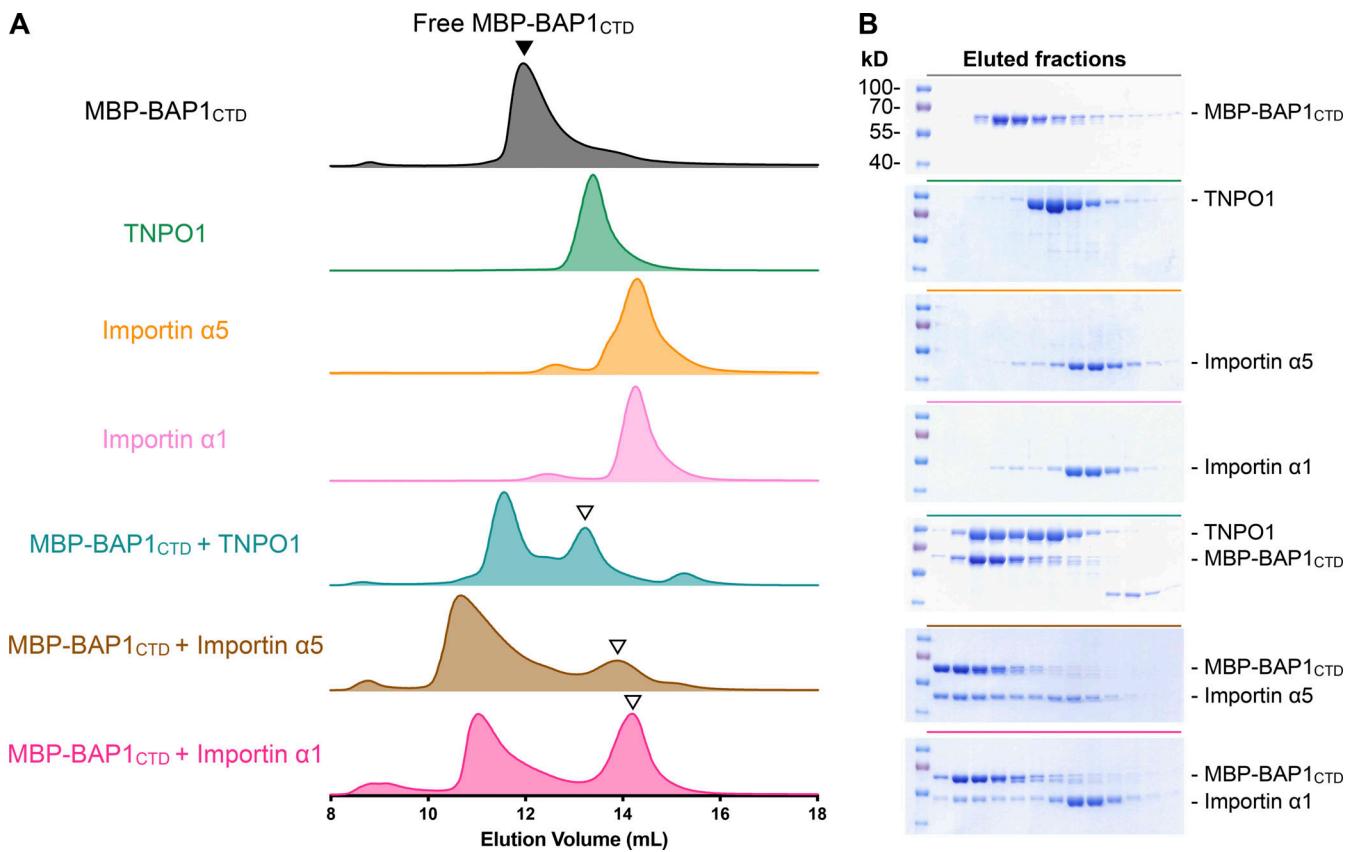
Figure 2. Physical interactions between BAP1 and TNPO1, importin α5, and importin α1. (A) SECs of free MBP-BAP1$_{CTD}$ (gray, black closed triangle), TNPO1 (green), importin α5 (orange), importin α1 (light pink), and MBP-BAP1$_{CTD}$ preincubated with TNPO1 (cyan), importin α5 (brown), and importin α1 (dark pink) in descending order. Free MBP-BAP1$_{CTD}$ was mixed with excess TNPO1, importin α5, and importin α1, resulting in the elution peak of binary complex at earlier elution volume and a lagging one that corresponds to the free nuclear import factor (open triangle). **(B)** SDS-PAGE analyses of the compositions of the elution peaks. The gels were stained with Coomassie blue. Source data are available for this figure: SourceData F2.

could mediate homodimerization of BAP1 (Fig. S2; Foglizzo et al., 2018). SEC-MALS analysis of isolated TNPO1 was strictly monomeric, with a mol wt of 91.2 ± 5.1 kD (the theoretical mol wt is 98.1 kD). Preincubation of MBP-BAP1$_{CTD}$ with TNPO1 showed an increased apparent mol wt of 136.2 ± 8.1 kD for the main elution peak, which corresponded to a 1:1 binary complex (Fig. 5 B). The results illustrated the ability of TNPO1 to dissociate homodimeric MBP-BAP1$_{CTD}$ to form a heterodimeric TNPO1:MBP-BAP1$_{CTD}$ complex with a 1:1 binding stoichiometry.

TNPO1 regulates the UBE2O-dependent mUb of BAP1

To investigate the structural basis of how TNPO1 targets BAP1, we crystallized TNPO1 in complex with the residues 706–724 of BAP1 harboring the PY-NLS (hereafter BAP1$_{PY-NLS}$) and solved the crystal structure to a resolution of 3.7 Å (Table 1). TNPO1 is composed of 20 HEAT repeats forming a superhelical architecture (Chook and Blobel, 1999; Cansizoglu and Chook, 2007; Lee et al., 2006). Each HEAT repeat comprises two antiparallel α-helices (Fig. S3 A). The crystal structure of the TNPO1: BAP1$_{PY-NLS}$ complex illustrated how HEAT repeats 8–12 (ranging from residues 300–550) of TNPO1 form a crevice to accommodate BAP1$_{PY-NLS}$ (Fig. 6, A and B; and Fig. S3 B). The proline-tyrosine residues (P723 and Y724) of BAP1 made extensive contacts with the hydrophobic swath of TNPO1 encompassing

residues A380, A381, L419, A425, I457, and W460 (Fig. 6 B). The refined structural model showed that R720 of BAP1 could participate in tripartite interactions with the side chains of T506, E509, and D543 of TNPO1. Additionally, the side chain hydroxyl group of S721 of BAP1 could be hydrogen bonded to the side chain of E498 of TNPO1 (Fig. 6 B). Due to the intrinsic disorder of the flanking residues of BAP1$_{PY-NLS}$, including K711, K714, K725, and K727 that have been reported to be monoubiquitinated by UBE2O (Mashtalir et al., 2014), their atomic structures could not be resolved in the crystal structure (Fig. 6 A). Nevertheless, their close proximity to the PY-NLS motif that was deeply buried inside the TNPO1 crevice suggests these mUb sites would be sterically sequestered by TNPO1 binding (Fig. 6, A and B).

To test whether TNPO1 binding interferes with the mUb of the NLS of BAP1, we generated recombinant UBE2O to establish an in vitro mUb assay with residues 699–729 of BAP1 (hereafter BAP1$_{699–729}$), which include the VLI patch and PY-NLS motif (Fig. 6 C). The use of fluorescein-labeled WT ubiquitin (fluorescein-Ub$_{WT}$) and the K0 ubiquitin mutant, in which all seven endogenous lysine residues are replaced by arginine residues (fluorescein-Ub$_{K0}$), resulted in similar ubiquitin ladders resolved by SDS-PAGE (Fig. S4), indicating that the multiple bands corresponded to different numbers of mUb sites rather than different lengths of polyubiquitin on a single ubiquitination site.
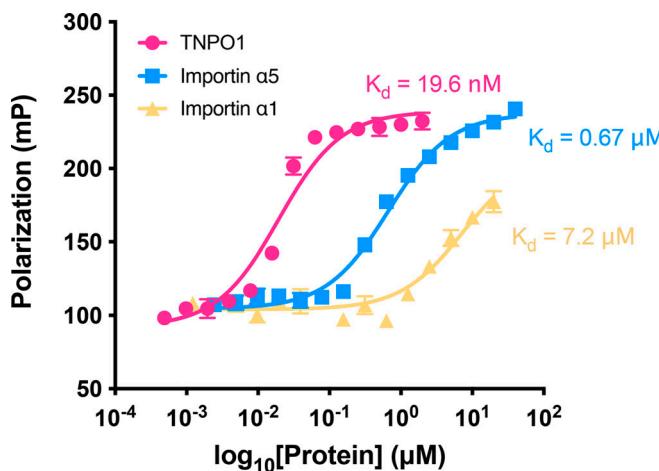
Figure 3. Functional assessment of BAP1 binding to TNPO1. TNPO1 exhibits the strongest binding affinity to BAP1 NLS among three import factors. K_d values were derived from the FP analyses as a function of binding protein concentration by fitting to a one-site binding model. Error bars are indicated as 95% confidence intervals based on technical triplicates ($n = 3$).

Site-specific MS analysis within the NLS2 was hampered by the abundance of arginine (R) and lysine (K) residues within this segment, resulting in short and redundant peptide digests, as trypsin and Arg-C both recognize the R and K for proteolysis. Nevertheless, we could observe up to four of the five lysine residues (K711, K714, K719, K725, and K727) within the $BAP1_{699-729}$ peptide that were monoubiquitinated by in-gel fluorescence imaging of the monoubiquitinated products (Fig. S4). Having established the multi-mUb of $BAP1_{699-729}$ by UBE2O, we asked whether TNPO1 binding to $BAP1_{699-729}$ would down-regulate the ubiquitin ligase activity of UBE2O. Preincubation of the FITC-labeled $BAP1_{699-729}$ with one or two molar ratios of TNPO1 for

1 h before initiating the mUb by UBE2O resulted in a substantially reduced level of multi-mUb of $BAP1_{699-729}$ in a TNPO1 dose–dependent manner (Fig. 6, E–G; and Fig. S5). Our structural and biochemical findings collectively demonstrated that TNPO1 binding to the NLS of BAP1 renders the mUb by UBE2O, which has direct implications in promoting BAP1 nuclear localization.

Discussion

DUB activity and nuclear localization are essential for the tumor suppressor activity of BAP1 (Ventii et al., 2008; Zhang et al., 2018). Although BAP1 is the first reported nuclear UCH, the molecular basis by which its nuclear import is regulated remains sparsely understood. The presence of the two putative NLS motifs, namely the monopartite classical NLS1 and the bipartite classical NLS2, suggests that nuclear import of BAP1 is potentially mediated by the canonical importin α/β system. Nonetheless, a nonclassical PY-NLS motif within the NLS2 reveals the implication of TNPO1 as an alternative nuclear import route. In this study, we demonstrated by comparative analysis of the subcellular localization of $BAP1_{WT}$ and $BAP1_{Q684*}$ that the NLS2, but not the NLS1, is responsible for nuclear import (Fig. 1, B and C). Through immunoprecipitation using transiently expressed BAP1 as bait, potential BAP1-binding proteins were identified by subsequent MS-based proteomic analysis. In particular, we identified importin α1, importin α5, and TNPO1 as prominent BAP1 nuclear import factors. Their physical interactions with BAP1 were verified by SEC, and their binding affinities to BAP1 were quantified by FP measurements, which established the strongest binding affinity of TNPO1 to the BAP1 NLS compared with importin α1 and α5 (Figs. 2 and 3). Importantly, the immunofluorescence imaging of karyopherin-KO cells led us to conclude that BAP1 nuclear import is chiefly regulated by TNPO1 (Fig. 4).
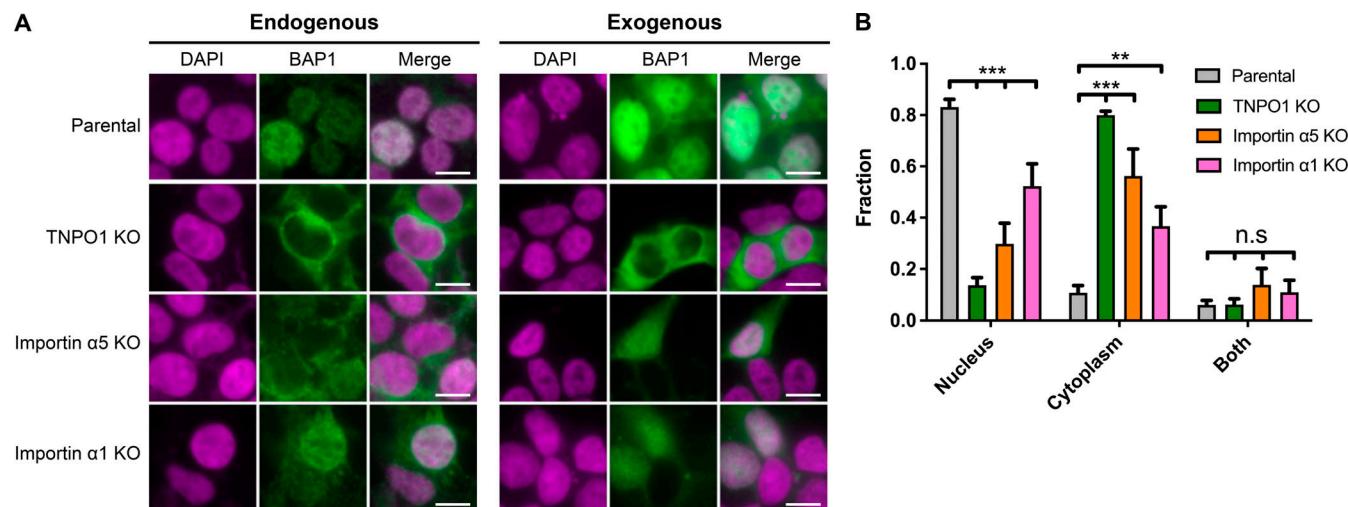
Figure 4. TNPO1 is the main regulator of BAP1 nuclear import. (A) Immunofluorescence of subcellular localization of endogenous BAP1 or ectopically expressed SNAP-tag fused BAP1 in TNPO1-, KPNA1 (encoding importin α5)-, and KPNA2 (importin α1)-KO cells. Scale bar = 10 μm. **(B)** Quantitative analysis of the nuclear/cytoplasmic fraction of ectopically expressed BAP1 in TNPO1-, KPNA1-, and KPNA2-KO HEK293 cells. The bar chart shows the mean and SEM of three independent experiments, counting ~250 cells in each experiment; data analyzed by two-way ANOVA and processed to multiple comparisons using Bonferroni posttest. **, adjusted $P < 0.01$; ***, adjusted $P < 0.001$ from two-way ANOVA and Bonferroni posttest.
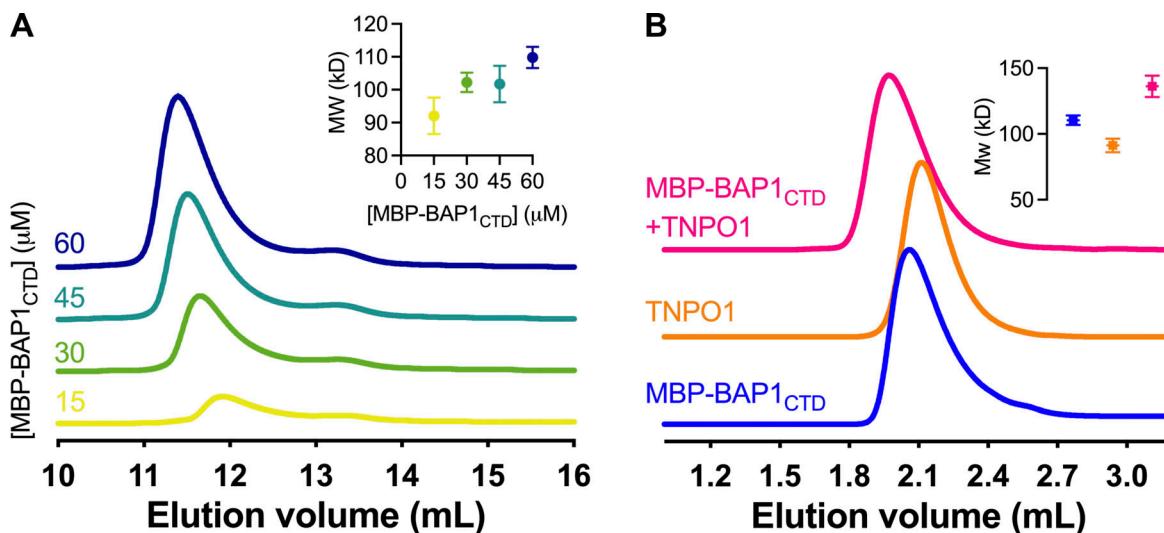
Figure 5. **TNPO1 regulates the CTD-mediated dimerization of BAP1. (A)** SEC-MALS analysis of free MBP-BAP1$_{CTD}$ as a function of protein concentration. **(B)** Binary complex formation between MBP-BAP1$_{CTD}$ and TNPO1. The SEC-MALS analyses of the binary complex, free TNPO1, and free MBP-BAP1$_{CTD}$ are shown in descending order. The mol wt values derived from SEC-MALS are shown in insets.

UBE2O is an atypical E2/E3 hybrid ubiquitin-conjugating enzyme (Berleth and Pickart, 1996; Ullah et al., 2019). UBE2O is reported to primarily monoubiquitinate the NLS region of BAP1 by recognizing a conserved patch of aliphatic hydrophobic amino acids, known as the VLI patch, leading to the cytoplasmic sequestration of BAP1 (Mashtalir et al., 2014). Indeed, UBE2O was found to associate with BAP1 in our affinity purification (AP)-MS analysis (Table S1), in line with previous reports (Sowa et al., 2009; Hauri et al., 2016; Mashtalir et al., 2014). The underlying mechanism of cytoplasmic retention of BAP1 was considered to result from the ubiquitination-mediated nuclear export (Mashtalir et al., 2014). However, several lines of evidence indicate that UBE2O primarily localizes in the cytoplasm (Sen Nkwe et al., 2020; Chen et al., 2018; Mashtalir et al., 2014). Since UBE2O harbors two functional NLS signals, Mashtalir et al. (2014) suggested that the mUb of the BAP1 NLS within the nucleus might be mediated by a small portion of UBE2O in the nucleus. In addition, they found that the mUb of BAP1 can be reverted by the auto-deubiquitination of BAP1 (Mashtalir et al., 2014). Hence, the opposing functions of UBE2O-mediated mUb and auto-deubiquitination activity of BAP1 require delicate spatial and temporal regulations in the context of the ubiquitination-mediated BAP1 nuclear export. Considering the predominantly cytoplasmic distribution of UBE2O that can monoubiquitinate cytoplasmic BAP1, thereby affecting its nuclear import (Mashtalir et al., 2014), our mUb assay provides strong evidence to indicate the dominant role of TNPO1 in suppressing the function of UBE2O and facilitating the nuclear import of BAP1 (Fig. 6). The crystal structure of TNPO1 in complex with BAP1$_{PY-NLS}$ provided the structural basis of how the PY-NLS motif of BAP1 is recognized by TNPO1 and how the complex formation results in steric hindrance to prevent UBE2O-mediated mUb of BAP1 NLS (Fig. 6).

In summary, we verified and demonstrated the essential role of TNPO1 in regulating the nuclear import of BAP1 by CRISPR/Cas9-based KO study (Figs. 1 and 4). We provided the structural basis of how TNPO1 recognizes BAP1 through binding to the atypical PY-NLS motif within its CTD (Figs. 2, 3, 4, 5, and 6). TNPO1 dissociates the CTD-mediated dimerization of BAP1 to form a stable binary complex (Fig. 5). Upon complex formation, TNPO1 sterically prevents UBE2O from monoubiquitinating the NLS of BAP1 (Fig. 6). This work therefore sheds light on the mechanism by which TNPO1 governs the nuclear import of the important tumor suppressor BAP1 to execute its function of transcription regulation.

Materials and methods

Molecular cloning, protein expression, and purification
The open reading frames of BAP1 and UBE2O were obtained from Addgene (pDEST-FLAG-HA-BAP1, plasmid #22539, and pcDNA3.1 3xFLAG-TEV-UBE2O, plasmid #105718). A cancer-associated nonsense mutation Q684* (residues 1–683) was generated with specific primers: forward, 5′-AATTGGATCCGCCAC CATGGACTACAAGGATGACG-3′; and reverse, 5′-AATTGCGGC CGCTTATTAAGCCAGCATGGAGATAAAGGT-3′.

The DNA sequences corresponding to individual BAP1 constructs were subcloned into the pcDNA3.4_TOPO expression vector (Invitrogen) with a FLAG-tag at the N-terminus for purification. The cancer-associated nonsense mutation, Q684*, is documented in the Catalogue of Somatic Mutations in Cancer (COSMIC, https://cancer.sanger.ac.uk/cosmic) and cBioPortal (https://www.cbioportal.org).

The plasmids corresponding to the BAP1 variants and UBE2O were individually transfected into HEK293 freestyle cells (Invitrogen) with polyethylenimine (linear, 25 kD; Polysciences) at a DNA/polyethylenimine ratio of 1:2. The transfected cells were incubated at 37°C and 8% CO_2 for 48–72 h. The cells were lysed using a Dounce homogenizer (Wheaton) in 50 mM Tris-HCl, pH 7.6, 150 mM NaCl, 0.1% IEGAL CA-630 (Sigma-Aldrich), and

Table 1. Data collection and refinement statistics (molecular replacement)

	TNPO1 in complex with BAP1$_{PY-NLS}$ (Protein Data Bank accession no. 7VPW)
Data collection	
Space group	$P22_12_1$
Cell dimensions	
a, b, c (Å)	68.90, 129.69, 170.21
α, β, γ (°)	90.00, 90.00, 90.00
Resolution (Å)	103.158–3.763
R_{merge}	0.1602 (1.24)[a]
$I/\sigma I$	7.33 (2.54)
Completeness (%)	98.79 (94.43)
Redundancy	7.2 (7.2)
Refinement	
Resolution (Å)	63.863–3.763 (3.897–3.763)
No. reflections	15,849 (1,472)
R_{work}/R_{free}	0.2293/0.2584
No. atoms	
Protein	6,705
B-factors	
Protein	87.26
Root mean square deviations	
Bond lengths (Å)	0.004
Bond angles (°)	0.805
MolProbity score	1.38
Clashscore	3.26
Ramachandran plot	
Favored (%)	96.17
Allowed (%)	3.83
Outliners (%)	0

[a]Statistics for the highest-resolution shell are shown in parentheses.

1 mM PMSF with 25–30 strokes. The cell lysate was filtered through a 0.22-μm cutoff membrane and incubated with anti-FLAG M2 antibody resins (Sigma-Aldrich) at 4°C for 4 h. The resins were iteratively washed with a wash buffer (50 mM Tris-HCl, pH 7.6, and 150 mM NaCl). The target protein was eluted with 50 mM Tris-HCl, pH 7.6, 150 mM NaCl, and 300 ng/μl 3× FLAG peptide. All recombinant proteins were concentrated and loaded into a SEC column (superpose 6 increase 10/300 GL; GE Healthcare) in SEC buffer (50 mM Tris-HCl , pH 7.6, 200 mM NaCl, 10% [vol/vol] glycerol, 0.2 mM tris(2-carboxyethyl)phosphine, 2 mM Mg[OAc]$_2$, and 1 mM EGTA).

The CTD (residues 596–729) of BAP1 was subcloned into the pET-MBP vector, which encodes for a His$_6$-MBP fusion tag at the N-terminus, followed by a TEV protease cleavage site for tag removal (hereafter His$_6$-MBP-BAP1$_{CTD}$): forward, 5′-AATTGG ATCCGGAAAACCTGTATTTTCAGGGCGGCAGCAGCAGCCCAG TGGAGAAG-3′; and reverse, 5′-AATTCTCGAGTTATCACTGGC GCTTGGCC-3′. Full-length TNPO1 (also known as Kapβ2) was a kind gift of Dr. Yuh Min Chook (University of Texas Southwestern Medical Center at Dallas, Dallas, TX). An acidic loop corresponding to residues 337–367 was replaced by a GGSGGSG linker for optimized crystallization (Yoshizawa et al., 2018).

Specific primers for In-Fusion HD Cloning kit, Takara Bio, were forward, 5′-TGGTTCTGGCGGCTCTGGTGATACAATTTC TGACTGGAATC-3′; and reverse, 5′-GAGCCGCCAGAACCACCC CGTATATCCTGTTCACTATCAG-3′.

Full-length importin α5 and importin α1 were obtained from Addgene (pCMVTNT-T7-KPNA1/plasmid #26677 and pCMVTNT-T7-KPNA2/plasmid #26678). The N-terminal importin β-binding (IBB) domains of importin α1 and α5 were excluded from the recombinant protein expression constructs, as the IBB domain is not required for cargo recognition.

For KPNA1 (importin α5, residues 66–512): forward-1, 5′-GGG CGGCAGCGAAGAAGAAACAGAAGAAGAAGTTATGTCAGATGG-3′; forward-2, 5′-AATTGGATCCGAAAACCTGTATTTTCAGGGCG GCAGCGAAGAAG-3′; reverse-1, 5′-AATTCTCGAGTCAAATAAGA TCAAAGGCCTTTTGGTAGATCTCC-3′; and reverse-2, 5′-AAT TGCGGCCGCTCAAATAAGATCAAAGGCCTTTTGGTAGATCT-3′.

For KPNA2 (importin α1, residues 60–529): forward-1, 5′-CAGGGCGGCAGCCTGAAGAGGAGAAATGTAAGCTCATTTCC-3′; forward-2, 5′-AATTGGATCCGAAAACCTGTATTTTCAGGGCGG CAGCCTG-3′; reverse-1, 5′-AATTCTCGAGTCAGAAAGTGTAGC CTTCAGAGGTAG-3′; reverse-2, 5′-AATTGCGGCCGCTCAGAA AGTGTAGCCTTCAGAGGTAG-3′.

They were subcloned into the pGEX-4T3 vector for recombinant protein expression. All nuclear import factors were fused with an N-terminal GST tag followed by a TEV cleavage site. His$_6$-MBP-BAP1$_{CTD}$, GST-TNPO1, and GST-importin-αs were expressed in E. coli strain BL21(DE3). All cultures were grown to OD$_{600}$ = 0.4–0.6, and expression was induced with 0.1 mM IPTG at 16°C for 20 h.

A tandem purification strategy was used for His$_6$-MBP-BAP1$_{CTD}$ purification. First, the cells were lysed in 50 mM Tris-HCl, pH 7.6, 1 M NaCl, 10% (vol/vol) glycerol, and 0.2 mM TCEP. After centrifugation, the supernatant was loaded into a MBPTrap HP 5 ml column (GE Healthcare), and target protein was eluted by the same buffer with 10 mM maltose. Next, the eluted sample was further purified by a HisTrap HP 5-ml column (GE Healthcare) in 50 mM Tris-HCl, pH 7.6, 1 M NaCl, 10% (vol/vol) glycerol, and 0.2 mM TCEP and eluted with elution buffer (50 mM Tris-HCl, pH 7.6, 1 M NaCl, 10% (vol/vol) glycerol, 0.2 mM TCEP, and 400 mM imidazole).

For GST-tagged import factors, the cells were lysed in 50 mM Tris-HCl (pH 7.6), 200 mM NaCl, 20% (vol/vol) glycerol, 0.2 mM TCEP, and 1 mM EDTA. Cell lysates were incubated with Glutathione Sepharose 4B resin (GE Healthcare) at 4°C for 4 h. On-column digestion for removing the GST-tag was achieved by TEV protease at room temperature for 2 h. Tag-free recombinant import factors were collected in the flow-through. His$_6$-MBP-BAP1$_{CTD}$ and untagged import factors were subsequently purified by SEC using a Superdex 200 16/60 GL column (GE Healthcare) in 50 mM Tris-HCl (pH 7.6), 150 mM NaCl, 10%

Yang et al.
BAP1 nuclear import is governed by TNPO1

Journal of Cell Biology   7 of 13
https://doi.org/10.1083/jcb.202201094
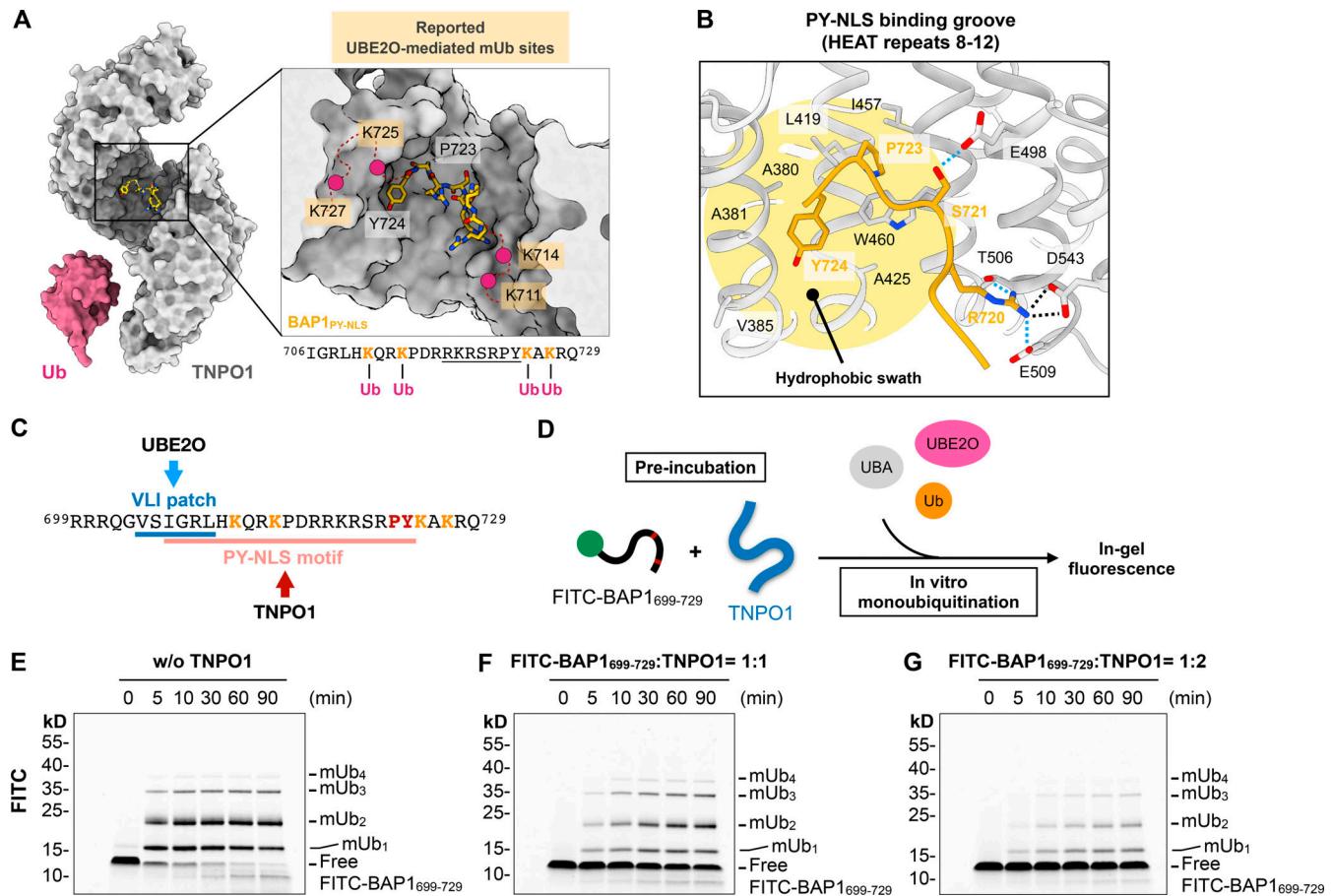
Figure 6. **TNPO1 sterically antagonizes UBE2O-mediated mUb of BAP1. (A)** Crystal structure of TNPO1 in complex with BAP1$_{PY-NLS}$. Due to the intrinsic flexibility, only residues 718–724 were resolved, shown in sticks (highlighted by underlining). The position of four lysine residues reported to be mono-ubiquitinated by UBE2O are tentatively indicated by pink spheres linked by a dashed line. Ub, ubiquitin. **(B)** Zoomed-in view of the PY-NLS binding groove of TNPO1 revealing the interaction between TNPO1 and BAP1$_{PY-NLS}$. The highlighted region colored in yellow represents the hydrophobic swatch in the HEAT repeats 8–12 of TNPO1, which accommodates the proline-tyrosine residues (^{723}PY^{724}) of BAP1$_{PY-NLS}$. The dashed lines indicate salt bridge (black) and hydrogen bond (light blue). **(C)** Overlapping binding motifs of UBE2O and TNPO1 within the NLS region of BAP1 (residues 699–729). Reported mUb sites are in orange. **(D)** Schematic representation of TNPO1 competition assay design. **(E–G)** In vitro mUb assays of FITC-labeled BAP1$_{699-729}$ peptide in the absence (E) and presence of one equivalent (F) and two equivalents (G) of TNPO1. Detection of mUb was visualized by in-gel fluorescence. Source data are available for this figure: SourceData F6.

(vol/vol) glycerol, 0.2 mM TCEP, 2 mM Mg(OAc)$_2$, and 1 mM EGTA. The purity of the recombinant proteins was confirmed by SDS-PAGE.

Subcellular localization and phenotypic profiling of BAP1 variants

HeLa-Kyoto cells were regularly maintained in DMEM with 10% FBS and 1% penicillin/streptomycin and plated in the chamber-slide (μ-Slide; Ibidi) before transfection. The DNA sequences corresponding to BAP1 variants were subcloned into the pSNAP-tag vector, with an N-terminal SNAP-tag for fluorescence labeling.

Plasmids of SNAP-tagged BAP1 variants were transfected into cells using X-tremeGENE HP reagent (Roche). 2 d after transfection, exogenous SNAP-tagged BAP1s were live-labeled with SNAP-Cell TMR-star (New England BioLabs), and nuclei were stained with Hoechst33342 (Thermo Fisher Scientific) for 30 min. Labeled cells were transferred into the fresh medium

and used for epifluorescent live-cell microscopy. Images were taken using a Leica DMI6000 microscope with an HCX PL FL 20×/0.40-NA CORR objective lens and an Andor Luca R EMCCD sensor. Integral fluorescent intensities of labeled BAP1 variants in the separate cellular compartments were processed and counted based on double-stained monochrome images using MetaMorph Multi-Wavelength cell scoring software application (Molecular Devices).

Immunofluorescence staining of exogenous and endogenous BAP1

For detecting endogenous BAP1, parental, *TNPO1*-, *KPNA1*-, and *KPNA2*-KO lines were fixed with 4% formalin, stained with mouse anti-BAP1 antibody (1:100, clone #C-4, sc-28383; Santa Cruz Biotechnology), and anti-mouse Alexa Fluor 594 antibody (1:2,000, A21203; Invitrogen), and mounted in DAPI-containing mounting medium (AB104139; Abcam). For detecting exogenous BAP1, HEK293T cells were transfected with SNAP-tagged BAP1

Yang et al.
BAP1 nuclear import is governed by TNPO1

Journal of Cell Biology 8 of 13
https://doi.org/10.1083/jcb.202201094

using X-tremeGENE HP reagent (Roche) for 2 d, and SNAP-tagged BAP1s were live-labeled with SNAP-Cell TMR-star (New England BioLabs) overnight. Labeled cells were fixed with 4% formalin and mounted in DAPI-containing mounting medium (Abcam). Immunofluorescence images were taken using a Leica DMI6000 microscope with an HCX PL FL 63×/1.4-NA objective lens and an Andor Luca R EMCCD sensor. Image acquisition was performed with the application of MetaMorph Multi-Wavelength acquisition software (Molecular Devices). Phenotypic distribution of BAP1 was manually counted in three independent assays, with ≥250 cells counted in each experiment.

Cas9 ribonucleoprotein (RNP) nucleofection

Recombinant Cas9 protein and sgRNA were prepared as previously described (Huang et al., 2021). Briefly, the plasmid pMJ915 (plasmid #69090; Addgene), encoding recombinant *Streptococcus pyogenes* Cas9, was transformed into *E. coli* strain BL21(DE3) for protein expression by IPTG induction. The Cas9 protein was first purified from *E. coli* lysate using an Ni-NTA affinity column. After removing the N-terminal His_6-MBP-tag with TEV protease, the untagged Cas9 protein was purified by ion exchange chromatography using a Heparin column, followed by SEC using a Superdex 200 16/60 gel filtration column. The purified Cas9 protein was stored in Cas9 RNP buffer (20 mM Hepes, 150 mM KCl, 10% glycerol, and 1 mM β-mercaptoethanol, pH 7.5). sgRNAs were synthesized from DNA templates by in vitro transcription using T7 polymerase and were purified by electrophoresis in urea-PAGE to extract the full-length sgRNA. sgRNAs were then treated with calf intestinal alkaline phosphatase to remove the immunogenic 5′ triphosphate moiety to reduce intracellular immune response (Wienert et al., 2018; Kim et al., 2018). Each target gene was disrupted by a double-cutting strategy in which two Cas9 RNP complexes were co-introduced to induce two double-strand breaks in the gene coding region. The sgRNA target sequences are as follows: *KPNA1* KO sgRNA-1, 5′-CCACTGTACTCCAGTCCGGG-3′; *KPNA1* KO sgRNA-2, 5′-ATCCCGATGAGATGCGCAGG-3′; *KPNA2* KO sgRNA-1, 5′-TCAGCCCTTTAGAGGGAAGG-3′; *KPNA2* KO sgRNA-2, 5′-TTGGAAGGGGTGAAAACTG-3′; *TNPO1* KO sgRNA-1, 5′-AGGAAAATTGCTGCCTGGGT-3′; and *TNPO1* KO sgRNA-2, 5′-CCCGGCCGTTTGAAGCCGAG-3′.

BFP-derived 127-bp single-stranded oligodeoxynucleotides (ssODNs) were prepared by dissolving Ultramer DNA Oligo (Integrated DNA Technologies) in molecular-grade water and adjusted to 100 µM for editing enhancement (Richardson et al., 2016). HEK293T cells were subcultured for 48 h before nucleofection. Cas9 RNP was assembled by swirling mixing Cas9 protein into sgRNA solution followed by incubation at 37°C for 15 min (Huang et al., 2021). The double-cut Cas9 RNP mixture was defined as 20 µM and prepared by combining an equal amount of sgRNA-1 and sgRNA-2 Cas9 RNP. All nucleofection experiments were performed using the 4D-Nucleofector X Unit (Lonza). Each nucleofection reaction contained 2×10^5 cells in 20 µl of nucleofection buffer, 5 µl of double-cut Cas9 RNP mixture, and 1 µl of 100 µM BFP-derived 127-bp ssODN. The HEK293T cells were pulsed with SF kit (Lonza) using the

program CM-130. After nucleofection, the pulsed cells were allowed to recover in the prewarmed medium at 37°C for 5 min and transferred to 6-well plates for subsequent analysis.

Genomic PCR amplification and editing analysis

The pulsed cells were harvested 48 h after nucleofection. The cells were pelleted at 300 *g* for 5 min, washed once with DPBS, and resuspended in QuickExtract DNA Extraction Solution (Lucigen). Genomic DNA extraction was performed at 65°C for 15 min, 98°C for 5 min, and on ice for 10 min. The following primers were used for genomic PCR: *KPNA1* forward, 5′-CCAGCTACTCAGGAAACTGAAGTG-3′; *KPNA1* reverse, 5′-CAGCAACACTTTAGTGGTCACTTGTG-3′; *KPNA2* forward, 5′-GATGGAGTATGGAAAAAGAATGTAGAAG-3′; *KPNA2* reverse, 5′-GTTTTCCTGCAGCGGAGAAGTAGCATCATCAGG-3′; *TNPO1* forward, 5′-GAGTGCGAGCACTTGTGAG-3′; and *TNPO1* reverse, 5′-GCTTAACAGGCGAGGCAAAC-3′

The targeted loci were amplified from extracted genomic DNA by KAPA HiFi HotStart PCR Kit (KAPA Biosystems). PCR products were resolved by 2% TAE agarose gel, poststained with SYBR Safe DNA Gel Stain (Thermo Fisher Scientific), and visualized by iBright FL1000 imaging system (Thermo Fisher Scientific).

Establish homozygous gene KO HEK293T single cell clone

The cells were collected 48 h after nucleofection. The cells were pelleted at 300 *g* for 5 min, washed once with DPBS, and resuspended in ice-cold FACS buffer (DPBS supplemented with 2% FBS, 25 mM HEPES, and 0.5 mM EDTA) containing 0.1 µg/ml DAPI solution (Thermo Fisher Scientific). Resuspended cells were then passed through a 35-µm cell strainer and collected into a 5-ml polypropylene test tube on ice in the dark until sorting. FACS was performed using a FACSAria IIIu Cell Sorter (BD Biosciences) by the flow cytometry core facility at the Institute of Biomedical Sciences, Academia Sinica, Taiwan. Single cells were sorted into a 96-well plate cultivated in complete DMEM. 96-well plates were incubated at 37°C for ≥10 d until single-cell colonies were formed. Single-cell colonies were picked up and analyzed by genomic PCR amplification to check the KO results. Homozygous KO clones were then expanded and cryopreserved until further experiments.

SEC-MALS analysis

The absolute mol wt values of MBP-BAP1$_{CTD}$ and TNPO1 were determined by SEC-MALS using a Wyatt Dawn Heleos II MALS detector (Wyatt Technology Corp.) coupled to an AKTA Purifier UPC10 FPLC protein purification system (GE Healthcare) as described previously (Wang et al., 2015). 15 µl of each sample at a concentration of 2 mg/ml was injected and separated using an Agilent BioSEC3 size-exclusion column (Agilent). All experiments were performed in 50 mM Tris-HCl, pH 7.6, 200 mM NaCl, 10% (vol/olv) glycerol, 0.2 mM TCEP, 2 mM Mg(OAc)$_2$, and 1 mM EGTA at a flow rate of 0.3 ml/min. The protein concentrations of individual elution peaks in the SECs were derived from the observed refractive index as a function of elution volume by a refractive index detector (Wyatt Optilab T-rEX; Wyatt Technology Corp.). A standard refractive index increment

(d*n*/d*c*) value of 0.185 ml/g was used, and the buffer viscosity η = 1.0257 cP at 25°C was estimated using SEDNTERP (http://philo.rasmb.org/software/sednterp/). The reference refractive index of SEC buffer (1.3458 RIU) was determined by passing buffer through the reference cell.

In vitro mUb assay
In vitro mUb was conducted in a total volume of 100 µl mixture containing 50 mM Tris-HCl, pH 8.0, 150 mM NaCl, 10 mM MgCl$_2$, 2 mM DTT, 250 nM ubiquitin-activating enzyme UBE1, 50 µM ubiquitin/fluorescein-ubiquitin (Ub$_{WT}$ or Ub$_{K0}$), 5 µM purified recombinant UBE2O, and 5 µM BAP1 substrate (unlabeled BAP1$_{CTD}$, BAP1$_{699-729}$, or FITC-labeled BAP1$_{699-729}$). For unlabeled BAP1$_{CTD}$ and BAP1$_{699-729}$, the reaction was performed with a mixture of fluorescein-labeled ubiquitin and unlabeled ubiquitin at a ratio of 1:4. For FITC-labeled BAP1$_{699-729}$, unlabeled ubiquitin was used for the experiment.

For competition assay, FITC-labeled BAP1$_{699-729}$ was preincubated with TNPO1 at the molar ratio of 1:1 and 1:2 for 1 h, and used as the substrate for the following reactions. All reactions were performed with constant shaking at 32°C for 0, 5, 10, 30, 60, and 90 min. The reaction at each time point was quenched by mixing with the SDS-loading dye and boiled at 95°C for 3 min. In-gel fluorescence was visualized with an excitation wavelength of 495 nm and an emission wavelength of 525 nm (iBright FL1000; Thermo Fisher Scientific). Samples were also confirmed by Coomassie blue staining.

Protein in-solution digestion
The sample was reduced with 10 mM dithioerythreitol and 25 mM ammonium bicarbonate (ABC), followed by the denaturation with 8 M urea and 25 mM ABC, pH 8.5, at 37°C for 1 h. After reduction and denaturation, the sample was alkylated with 25 mM iodoacetamide and 25 mM ABC, pH 8.5, at room temperature in the dark for 1 h. The reaction was quenched in 25 mM dithioerythreitol and 25 mM ABC.

Protein digestion was accomplished in two steps by using Lys-C (mass spectrometry grade; Wako) for 3 h in 25 mM ABC, pH 8.5, and 4 M urea, and using trypsin (sequencing grade; Promega) for 16 h in 25 mM ABC, pH 8.5, and 1 M urea. The enzyme-to-protein ratio for both digestion processes was 1:50. The reaction was quenched with 0.1% formic acid, and the sample was subsequently dried in Speedvac. The peptide mixture was aliquoted, desalted, and concentrated on a C18-ZipTip (Millipore) and eluted with 50% acetonitrile in 0.1% formic acid.

Shotgun proteomic identifications
NanoLC-nanoESI-MS/MS analysis was performed on an EASY-nLC 1200 system connected to a Thermo Orbitrap Fusion Lumos mass spectrometer (Thermo Fisher Scientific) equipped with a Nanospray Flex ion source (Thermo Fisher Scientific). Peptide mixtures were loaded onto a 75-µm internal diameter, 25-cm length PepMap C18 column (Thermo Fisher Scientific) packed with 2-µm particles with a pore size of 100 Å and separated using a segmented gradient in 120 min from 5 to 45% solvent B (80% acetonitrile with 0.1% formic acid) at a flow rate of 300 nl/min. Solvent A was 0.1% formic acid in water. The mass spectrometer was operated in the data-dependent mode. Briefly, survey scans of peptide precursors from 350 to 1,600 *m/z* were performed at 240K resolution with a 2 × 10^5 ion count target.

Tandem MS was performed by isolation window at 1.6 D with the quadrupole, HCD fragmentation with a normalized collision energy of 30, and rapid scan MS analysis in the ion trap. The MS^2 ion count target was set to 1 × 10^4, and the max injection time was 35 ms. Only those precursors with charge states 2–6 were sampled for MS^2. The instrument was run in top speed mode with 3-s cycles; the dynamic exclusion duration was set to 15 s with a 10-ppm tolerance around the selected precursor and its isotopes. Monoisotopic precursor selection was turned on.

The raw data obtained from LC-MS/MS acquisition was processed using Proteome Discoverer (v2.4; Thermo Fisher Scientific). The processed data were used to search against the Swissprot *Homo sapiens* database using Mascot search engine (v2.7.0; Matrix Science). All searches included carbamidomethyl (cysteine) and oxidation (methionine) as variable modifications. Two missed tryptic cleavages were allowed. The product mass tolerance of the parent ions and the fragment ions was set to 10 ppm and 0.6 D, respectively. A decoy database search was performed. Identified peptides were filtered with 1% false discovery rate cutoff.

FP
The residues 699–729 of BAP1 were chemically synthesized, and FITC was introduced to the N-terminus with an AHX linker (FITC-AHX-^{699}RRRQGVSIGRLHKQRKPDRRKRSRPYKAKRQ^{729}). FP measurements were performed in a filter-based microplate reader (Infinite M1000; TECAN) using a fluorescein filter set with an excitation wavelength (λ_{ex}) of 485 nm and an emission wavelength (λ_{em}) of 535 nm. The total reaction volume was fixed to 100 µl containing a serial dilution of different nuclear import carriers (TNPO1, importin α1 and α5) and 50 nM of FITC-labeled BAP1$_{699-729}$. The reactions were carried out at 25°C in triplicate. K_d values were determined by nonlinear regression using the one site, total binding model in Prism 9 (GraphPad).

Crystallization, data collection, and structure determination
To form the BAP1:TNPO1 complex, 7 mg/ml of untagged TNPO1 was preincubated with recombinant BAP1$_{CTD}$ and two chemically synthesized NLS peptides of BAP1$_{699-729}$ and BAP1$_{PY-NLS}$ (residues 706–724) at a molar ratio of 1:5 in 50 mM Tris-HCl, pH 7.6, 200 mM NaCl, 10% (vol/vol) glycerol, 0.2 mM TCEP, 2 mM Mg(OAc)$_2$, and 1 mM EGTA, respectively. The excess of free BAP1 peptides was removed by a 10-kD cutoff Amicon centrifuge tube. The initial trial of crystallization was accomplished by automatic robot screening (Phoenix RE; Rigaku). Further optimization was manually operated using the sitting-drop vapor diffusion method at 20°C overnight. 1 µl of protein sample was mixed with the same equivalent of crystallization reservoir buffer (0.49 M sodium phosphate monobasic monohydrate and 0.91 M potassium phosphate dibasic monohydrate, pH 7.4). Plate-like crystals of the BAP1:TNPO1 complex were grown overnight and harvested for x-ray diffraction.

The best crystal of the BAP1$_{PY-NLS}$:TNPO1 complex was diffracted to 3.7 Å and indexed to the space group $P22_12_1$. The initial

structure was solved by the molecular replacement method with Phaser (McCoy et al., 2007), using the reported structure (TNPO1:JKTBP$_{NLS}$ complex, Protein Data Bank accession no. 2Z5O) as a searching template. The BAP1$_{PY-NLS}$ peptide ligand was manually modeled by Coot (Emsley et al., 2010), refined by ISOLDE (Croll, 2018) and Phenix (Adams et al., 2010), and validated by MolProbity (Chen et al., 2010). The final structure was refined to an R_{work} value of 0.2293 and an R_{free} value of 0.2584. The structural validation parameters are shown in Table 1. A missing fragment from residues 706–717 of BAP1 shows no electron densities in terms of structural flexibility and disorder. Structural visualization and rendering were accomplished by a combination of UCSF-ChimeraX (Goddard et al., 2018) and PyMOL (Schrödinger).

Statistical analysis

Data analyses were performed using GraphPad Prism 9. Unpaired, two-tailed t test was used to compare two groups, and $P < 0.05$ was considered statistically significant. Two-way ANOVA followed by the Bonferroni posttest was used for multiple comparisons. K_d values reported in Fig. 3 were derived from nonlinear regression fitting to a one-site binding model with error bars indicating 95% confidence intervals based on technical triplicates (n = 3).

Online supplemental material

Fig. S1 shows the CRISPR/Cas9-based genome editing strategy for and the results of generating three *TNPO1-*, *KPNA1-*, and *KPNA2*-KO cells. Fig. S2 shows the sequence alignment between human BAP1 and its *Drosophila* ortholog Calypso, which share a conserved C-terminal region. Fig. S3 illustrates expanded views of the crystal structure of TNPO1:BAP1$_{706-724}$ crystal structure. Fig. S4 shows the results of the in vitro UBE2O-mediated mUb with the BAP1 NLS peptide. Related to Fig. 6, Fig. S5 shows how TNPO1 impairs UBE2O-mediated mUb of BAP1 NLS peptide. Table S1 lists the BAP1-associated proteins identified by AP-MS.

Data availability

The atomic coordinates of TNPO1 in complex with the PY-NLS motif (residues 706–724) of BAP1 are deposited in Protein Data Bank under accession no. 7VPW. In addition, the AP-MS raw dataset of BAP1-associated proteins identification has been deposited to Proteomics IDEntifications Database (PRIDE, https://www.ebi.ac.uk/pride/) under accession code PXD030044.

Acknowledgments

References

Adams, P.D., P.V. Afonine, G. Bunkoczi, V.B. Chen, I.W. Davis, N. Echols, J.J. Headd, L.W. Hung, G.J. Kapral, R.W. Grosse-Kunstleve, et al. 2010. PHENIX: A comprehensive Python-based system for macromolecular structure solution. *Acta Crystallogr. Sect. D Biol. Crystallogr.* 66:213–221. https://doi.org/10.1107/S0907444909052925

Baymaz, H.I., A. Fournier, S. Laget, Z. Ji, P.W. Jansen, A.H. Smits, L. Ferry, A. Mensinga, I. Poser, A. Sharrocks, et al. 2014. MBD5 and MBD6 interact with the human PR-DUB complex through their methyl-CpG-binding domain. *Proteomics*. 14:2179–2189. https://doi.org/10.1002/pmic.201400013

Berleth, E.S., and C.M. Pickart. 1996. Mechanism of ubiquitin conjugating enzyme E2-230K: Catalysis involving a thiol relay? *Biochemistry*. 35:1664–1671. https://doi.org/10.1021/bi952105y

Bononi, A., C. Giorgi, S. Patergnani, D. Larson, K. Verbruggen, M. Tanji, L. Pellegrini, V. Signorato, F. Olivetto, S. Pastorino, et al. 2017. BAP1 regulates IP3R3-mediated Ca²⁺ flux to mitochondria suppressing cell transformation. *Nature*. 546:549–553. https://doi.org/10.1038/nature22798

Cansizoglu, A.E., and Y.M. Chook. 2007. Conformational heterogeneity of karyopherin beta2 is segmental. *Structure*. 15:1431–1441. https://doi.org/10.1016/j.str.2007.09.009

Carbone, M., H. Yang, H.I. Pass, T. Krausz, J.R. Testa, and G. Gaudino. 2013. BAP1 and cancer. *Nat. Rev. Cancer*. 13:153–159. https://doi.org/10.1038/nrc3459

Carbone, M., D. Shimizu, A. Napolitano, M. Tanji, H.I. Pass, H. Yang, and S. Pastorino. 2016. Positive nuclear BAP1 immunostaining helps differentiate non-small cell lung carcinomas from malignant mesothelioma. *Oncotarget*. 7:59314–59321. https://doi.org/10.18632/oncotarget.10653

Chen, V.B., W.B. Arendall 3rd, J.J. Headd, D.A. Keedy, R.M. Immormino, G.J. Kapral, L.W. Murray, J.S. Richardson, and D.C. Richardson. 2010.

MolProbity: All-atom structure validation for macromolecular crystallography. *Acta Crystallogr. Sect. D Biol. Crystallogr.* 66:12–21. https://doi.org/10.1107/S0907444909042073

Chen, S., J. Yang, Y. Zhang, C. Duan, Q. Liu, Z. Huang, Y. Xu, L. Zhou, and G. Xu. 2018. Ubiquitin-conjugating enzyme UBE2O regulates cellular clock function by promoting the degradation of the transcription factor BMAL1. *J. Biol. Chem.* 293:11296–11309. https://doi.org/10.1074/jbc.RA117.001432

Chook, Y.M., and G. Blobel. 1999. Structure of the nuclear transport complex karyopherin-beta2-Ran × GppNHp. *Nature.* 399:230–237. https://doi.org/10.1038/20375

Croll, T.I. 2018. ISOLDE: A physically realistic environment for model building into low-resolution electron-density maps. *Acta Crystallogr. Sect. D Biol. Crystallogr.* 74:519–530. https://doi.org/10.1107/S2059798318002425

Eletr, Z.M., and K.D. Wilkinson. 2011. An emerging model for BAP1's role in regulating cell cycle progression. *Cell Biochem. Biophys.* 60:3–11. https://doi.org/10.1007/s12013-011-9184-6

Emsley, P., B. Lohkamp, W.G. Scott, and K. Cowtan. 2010. Features and development of Coot. *Acta Crystallogr. Sect. D Biol. Crystallogr.* 66:486–501. https://doi.org/10.1107/S0907444910007493

Farquhar, N., S. Thornton, S.E. Coupland, J.M. Coulson, J.J. Sacco, Y. Krishna, H. Heimann, A. Taktak, C.M. Cebulla, M.H. Abdel-Rahman, and H. Kalirai. 2018. Patterns of BAP1 protein expression provide insights into prognostic significance and the biology of uveal melanoma. *J. Pathol. Clin. Res.* 4:26–38. https://doi.org/10.1002/cjp2.86

Foglizzo, M., A.J. Middleton, A.E. Burgess, J.M. Crowther, R.C.J. Dobson, J.M. Murphy, C.L. Day, and P.D. Mace. 2018. A bidentate polycomb repressive-deubiquitinase complex is required for efficient activity on nucleosomes. *Nat. Commun.* 9:3932. https://doi.org/10.1038/s41467-018-06186-1

Goddard, T.D., C.C. Huang, E.C. Meng, E.F. Pettersen, G.S. Couch, J.H. Morris, and T.E. Ferrin. 2018. UCSF ChimeraX: Meeting modern challenges in visualization and analysis. *Protein Sci.* 27:14–25. https://doi.org/10.1002/pro.3235

Harbour, J.W., M.D. Onken, E.D. Roberson, S. Duan, L. Cao, L.A. Worley, M.L. Council, K.A. Matatall, C. Helms, and A.M. Bowcock. 2010. Frequent mutation of BAP1 in metastasizing uveal melanomas. *Science.* 330:1410–1413. https://doi.org/10.1126/science.1194472

Hauri, S., F. Comoglio, M. Seimiya, M. Gerstung, T. Glatter, K. Hansen, R. Aebersold, R. Paro, M. Gstaiger, and C. Beisel. 2016. A high-density map for navigating the human polycomb complexome. *Cell Rep.* 17:583–595. https://doi.org/10.1016/j.celrep.2016.08.096

He, M., M.S. Chaurushiya, J.D. Webster, S. Kummerfeld, R. Reja, S. Chaudhuri, Y.J. Chen, Z. Modrusan, B. Haley, D.L. Dugger, et al. 2019. Intrinsic apoptosis shapes the tumor spectrum linked to inactivation of the deubiquitinase BAP1. *Science.* 364:283–285. https://doi.org/10.1126/science.aav4902

Huang, R.S., M.C. Lai, H.A. Shih, and S. Lin. 2021. A robust platform for expansion and genome editing of primary human natural killer cells. *J. Exp. Med.* 218:e20201529. https://doi.org/10.1084/jem.20201529

Jensen, D.E., M. Proctor, S.T. Marquis, H.P. Gardner, S.I. Ha, L.A. Chodosh, A.M. Ishov, N. Tommerup, H. Vissing, Y. Sekido, et al. 1998. BAP1: A novel ubiquitin hydrolase which binds to the BRCA1 RING finger and enhances BRCA1-mediated cell growth suppression. *Oncogene.* 16:1097–1112. https://doi.org/10.1038/sj.onc.1201861

Ji, Z., H. Mohammed, A. Webber, J. Ridsdale, N. Han, J.S. Carroll, and A.D. Sharrocks. 2014. The forkhead transcription factor FOXK2 acts as a chromatin targeting factor for the BAP1-containing histone deubiquitinase complex. *Nucleic Acids Res.* 42:6232–6242. https://doi.org/10.1093/nar/gku274

Jumper, J., R. Evans, A. Pritzel, T. Green, M. Figurnov, O. Ronneberger, K. Tunyasuvunakool, R. Bates, A. Zidek, A. Potapenko, et al. 2021. Highly accurate protein structure prediction with AlphaFold. *Nature.* 596:583–589. https://doi.org/10.1038/s41586-021-03819-2

Kalirai, H., A. Dodson, S. Faqir, B.E. Damato, and S.E. Coupland. 2014. Lack of BAP1 protein expression in uveal melanoma is associated with increased metastatic risk and has utility in routine prognostic testing. *Br. J. Cancer.* 111:1373–1380. https://doi.org/10.1038/bjc.2014.417

Kim, S., T. Koo, H.G. Jee, H.Y. Cho, G. Lee, D.G. Lim, H.S. Shin, and J.S. Kim. 2018. CRISPR RNAs trigger innate immune responses in human cells. *Genome Res.* 28:367–373. https://doi.org/10.1101/gr.231936.117

Klemperer, N.S., E.S. Berleth, and C.M. Pickart. 1989. A novel, arsenite-sensitive E2 of the ubiquitin pathway: Purification and properties. *Biochemistry.* 28:6035–6041. https://doi.org/10.1021/bi00440a047

Koopmans, A.E., R.M. Verdijk, R.W. Brouwer, T.P. Van Den Bosch, M.M. Van Den Berg, J. Vaarwater, C.E. Kockx, D. Paridaens, N.C. Naus, M. Nellist, et al. 2014. Clinical significance of immunohistochemistry for detection of BAP1 mutations in uveal melanoma. *Mod. Pathol.* 27:1321–1330. https://doi.org/10.1038/modpathol.2014.43

Lee, B.J., A.E. Cansizoglu, K.E. Suel, T.H. Louis, Z.C. Zhang, and Y.M. Chook. 2006. Rules for nuclear localization sequence recognition by karyopherin beta 2. *Cell.* 126:543–558. https://doi.org/10.1016/j.cell.2006.05.049

Machida, Y.J., Y. Machida, A.A. Vashisht, J.A. Wohlschlegel, and A. Dutta. 2009. The deubiquitinating enzyme BAP1 regulates cell growth via interaction with HCF-1. *J. Biol. Chem.* 284:34179–34188. https://doi.org/10.1074/jbc.M109.046755

Mashtalir, N., S. Daou, H. Barbour, N.N. Sen, J. Gagnon, I. Hammond-Martel, H.H. Dar, M. Therrien, and E.B. Affar. 2014. Autodeubiquitination protects the tumor suppressor BAP1 from cytoplasmic sequestration mediated by the atypical ubiquitin ligase UBE2O. *Mol. Cell.* 54:392–406. https://doi.org/10.1016/j.molcel.2014.03.002

McCoy, A.J., R.W. Grosse-Kunstleve, P.D. Adams, M.D. Winn, L.C. Storoni, and R.J. Read. 2007. Phaser crystallographic software. *J. Appl. Crystallogr.* 40:658–674. https://doi.org/10.1107/S0021889807021206

Misaghi, S., S. Ottosen, A. Izrael-Tomasevic, D. Arnott, M. Lamkanfi, J. Lee, J. Liu, K. O'rourke, V.M. Dixit, and A.C. Wilson. 2009. Association of C-terminal ubiquitin hydrolase BRCA1-associated protein 1 with cell cycle regulator host cell factor 1. *Mol. Cell. Biol.* 29:2181–2192. https://doi.org/10.1128/MCB.01517-08

Nishikawa, H., W. Wu, A. Koike, R. Kojima, H. Gomi, M. Fukuda, and T. Ohta. 2009. BRCA1-associated protein 1 interferes with BRCA1/BARD1 RING heterodimer activity. *Cancer Res.* 69:111–119. https://doi.org/10.1158/0008-5472.CAN-08-3355

Pan, H., R. Jia, L. Zhang, S. Xu, Q. Wu, X. Song, H. Zhang, S. Ge, X.L. Xu, and X. Fan. 2015. BAP1 regulates cell cycle progression through E2F1 target genes and mediates transcriptional silencing via H2A monoubiquitination in uveal melanoma cells. *Int. J. Biochem. Cell Biol.* 60:176–184. https://doi.org/10.1016/j.biocel.2015.01.001

Pumroy, R.A., and G. Cingolani. 2015. Diversification of importin-alpha isoforms in cellular trafficking and disease states. *Biochem. J.* 466:13–28. https://doi.org/10.1042/BJ20141186

Qin, J., Z. Zhou, W. Chen, C. Wang, H. Zhang, G. Ge, M. Shao, D. You, Z. Fan, H. Xia, et al. 2015. BAP1 promotes breast cancer cell proliferation and metastasis by deubiquitinating KLF5. *Nat. Commun.* 6:8471. https://doi.org/10.1038/ncomms9471

Richardson, C.D., G.J. Ray, N.L. Bray, and J.E. Corn. 2016. Non-homologous DNA increases gene disruption efficiency by altering DNA repair outcomes. *Nat. Commun.* 7:12463. https://doi.org/10.1038/ncomms12463

Robert, X., and P. Gouet. 2014. Deciphering key features in protein structures with the new ENDscript server. *Nucleic Acids Res.* 42:W320–W324. https://doi.org/10.1093/nar/gku316

Sahtoe, D.D., W.J. Van Dijk, R. Ekkebus, H. Ovaa, and T.K. Sixma. 2016. BAP1/ASXL1 recruitment and activation for H2A deubiquitination. *Nat. Commun.* 7:10292. https://doi.org/10.1038/ncomms10292

Sen Nkwe, N., S. Daou, M. Uriarte, J. Gagnon, N.V. Iannantuono, H. Barbour, H. Yu, L. Masclef, E. Fernandez, N. Zamorano Cuervo, et al. 2020. A potent nuclear export mechanism imposes USP16 cytoplasmic localization during interphase. *J. Cell Sci.* 133:jcs239236. https://doi.org/10.1242/jcs.239236

Sime, W., Q. Niu, Y. Abassi, K.C. Masoumi, R. Zarrizi, J.B. Kohler, S. Kjellstrom, V.A. Lasorsa, M. Capasso, H. Fu, and R. Massoumi. 2018. BAP1 induces cell death via interaction with 14-3-3 in neuroblastoma. *Cell Death Dis.* 9:458. https://doi.org/10.1038/s41419-018-0500-6

Sowa, M.E., E.J. Bennett, S.P. Gygi, and J.W. Harper. 2009. Defining the human deubiquitinating enzyme interaction landscape. *Cell.* 138:389–403. https://doi.org/10.1016/j.cell.2009.04.042

Testa, J.R., M. Cheung, J. Pei, J.E. Below, Y. Tan, E. Sementino, N.J. Cox, A.U. Dogan, H.I. Pass, S. Trusa, et al. 2011. Germline BAP1 mutations predispose to malignant mesothelioma. *Nat. Genet.* 43:1022–1025. https://doi.org/10.1038/ng.912

Twyffels, L., C. Gueydan, and V. Kruys. 2014. Transportin-1 and Transportin-2: Protein nuclear import and beyond. *FEBS Lett.* 588:1857–1868. https://doi.org/10.1016/j.febslet.2014.04.023

Ullah, K., E. Zubia, M. Narayan, J. Yang, and G. Xu. 2019. Diverse roles of the E2/E3 hybrid enzyme UBE2O in the regulation of protein ubiquitination, cellular functions, and disease onset. *FEBS J.* 286:2018–2034. https://doi.org/10.1111/febs.14708

Varadi, M., S. Anyango, M. Deshpande, S. Nair, C. Natassia, G. Yordanova, D. Yuan, O. Stroe, G. Wood, A. Laydon, et al. 2022. AlphaFold protein structure database: Massively expanding the structural coverage of protein-sequence space with high-accuracy models. *Nucleic Acids Res.* 50:D439–D444. https://doi.org/10.1093/nar/gkab1061

Ventii, K.H., N.S. Devi, K.L. Friedrich, T.A. Chernova, M. Tighiouart, E.G. Van Meir, and K.D. Wilkinson. 2008. BRCA1-associated protein-1 is a tumor suppressor that requires deubiquitinating activity and nuclear localization. *Cancer Res.* 68:6953–6962. https://doi.org/10.1158/0008-5472.CAN-08-0365

Wang, I., S.Y. Chen, and S.T. Hsu. 2015. Unraveling the folding mechanism of the smallest knotted protein, MJ0366. *J. Phys. Chem. B.* 119:4359–4370. https://doi.org/10.1021/jp511029s

Wienert, B., J. Shin, E. Zelin, K. Pestal, and J.E. Corn. 2018. In vitro-transcribed guide RNAs trigger an innate immune response via the RIG-I pathway. *PLoS Biol.* 16:e2005840. https://doi.org/10.1371/journal.pbio.2005840

Yoshizawa, T., R. Ali, J. Jiou, H.Y.J. Fung, K.A. Burke, S.J. Kim, Y. Lin, W.B. Peeples, D. Saltzberg, M. Soniat, et al. 2018. Nuclear import receptor inhibits phase separation of FUS through binding to multiple sites. *Cell.* 173:693–705.e22. https://doi.org/10.1016/j.cell.2018.03.003

Yu, H., N. Mashtalir, S. Daou, I. Hammond-Martel, J. Ross, G. Sui, G.W. Hart, F.J. Rauscher 3rd, E. Drobetsky, E. Milot, et al. 2010. The ubiquitin carboxyl hydrolase BAP1 forms a ternary complex with YY1 and HCF-1 and is a critical regulator of gene expression. *Mol. Cell. Biol.* 30:5071–5085. https://doi.org/10.1128/MCB.00396-10

Zhang, Y., J. Shi, X. Liu, L. Feng, Z. Gong, P. Koppula, K. Sirohi, X. Li, Y. Wei, H. Lee, et al. 2018. BAP1 links metabolic regulation of ferroptosis to tumour suppression. *Nat. Cell. Biol.* 20:1181–1192. https://doi.org/10.1038/s41556-018-0178-0
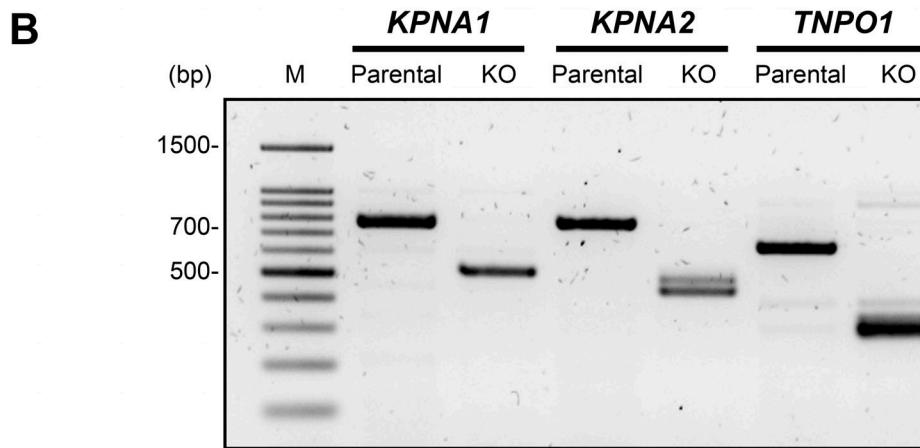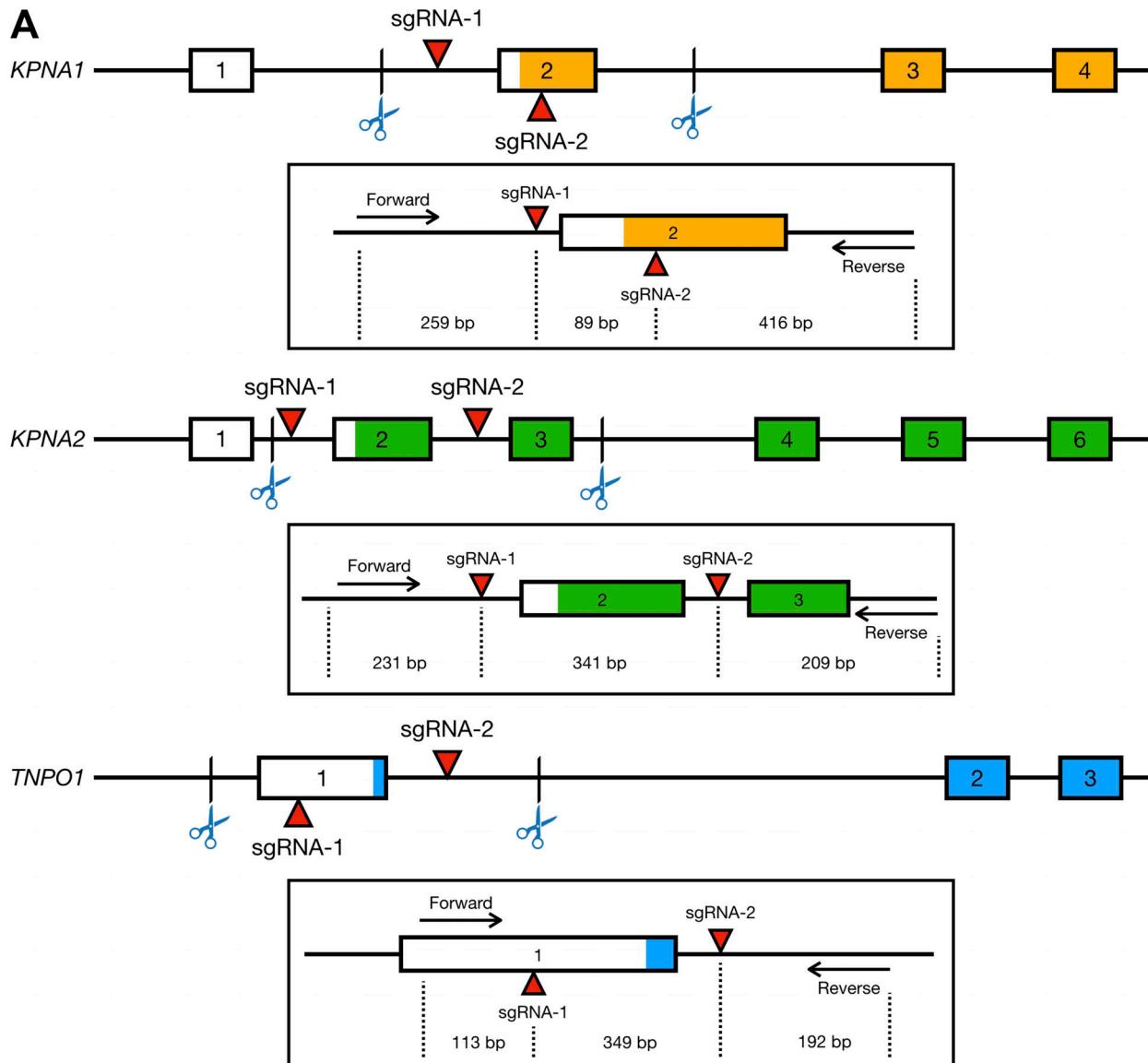
Supplemental material

Figure S1. **KO of TNPO1, importin α5, and importin α1 gene in HEK293 cells. (A)** Schematic illustration of CRISPR/Cas9-mediated genome editing of *KPNA1* (importin α5), *KPNA2* (importin α1), and *TNPO1* genes by introducing the double-cut KO strategy. The sgRNA target positions of each gene are indicated by red arrows. The insets indicate the expected sizes of PCR fragments generated by specific forward/reverse primers. **(B)** Detection of CRISPR-Cas9–dependent *KPNA1*, *KPNA2*, and *TNPO1* deletions, in comparison with the parental, was confirmed by PCR-based genotyping. Source data are available for this figure: SourceData FS1.

```
                                                              α8                                    α9
        οοοοοοοοοοοοοοοοοοοοοοοοοοοοοοοοοοοοοοοοοοοοοοοοοοοοοοοοοοοο              οοοοοοοοοοο
BAP1       624 GEKYSPKELLALLKCVEAEIANYEACLKEEVEKRKKFKIDDQRRTHNYDEFICTFISMLA
Calypso    329 PSAFTARDIQSLLKNLDTEIAINEQHLADENDRRHMFKVDASRRTHNYDKFICTFLSMLA
consensus>70   ...%...#L..LLK..#.EIA..E..L.#E.#.R..FK!D..RRTHNYD.FICTF.SMLA
```

```
               οο
BAP1       684 QEGMLANLVEQNISVRRR.QGV.SIGRLHKQR........................
Calypso    389 HQGVLGELVSQHLLPSKKVSGQGAANRISKQSTTASAGGSTAAGTASTPKTQQQQAAAAK
consensus>70   .#G.L.#LV.Q.........G.....R..KQ........................
```

```
BAP1       714 .......KPDRRKRSRPYKAKRQ
Calypso    449 NGKSPSKTPGRRKGRNKCRKRK
consensus>70   ........P.RR...R....KR.
```

Figure S2. **BAP1 and its *Drosophila* ortholog Calypso share a highly conserved C-terminal region.** Sequences of the C-terminal region of BAP1 and the *Drosophila* ortholog Calypso were aligned using T-coffee/Expresso and visualized by Esprit 3.0 (Robert and Gouet, 2014). Schematic representation of the secondary structure shown on the top of alignment corresponds to the solved structure of Calypso. The boxes in red indicate completely conserved residues, and boxes in yellow indicate the residues have similar physiochemical properties.

A

Y533
Y542
Y518

HEAT repeat of TNPO1
(Residues 518-557)

B

BAP1₇₀₆₋₇₂₄

PY-NLS binding groove
(HEAT repeats 8-12)
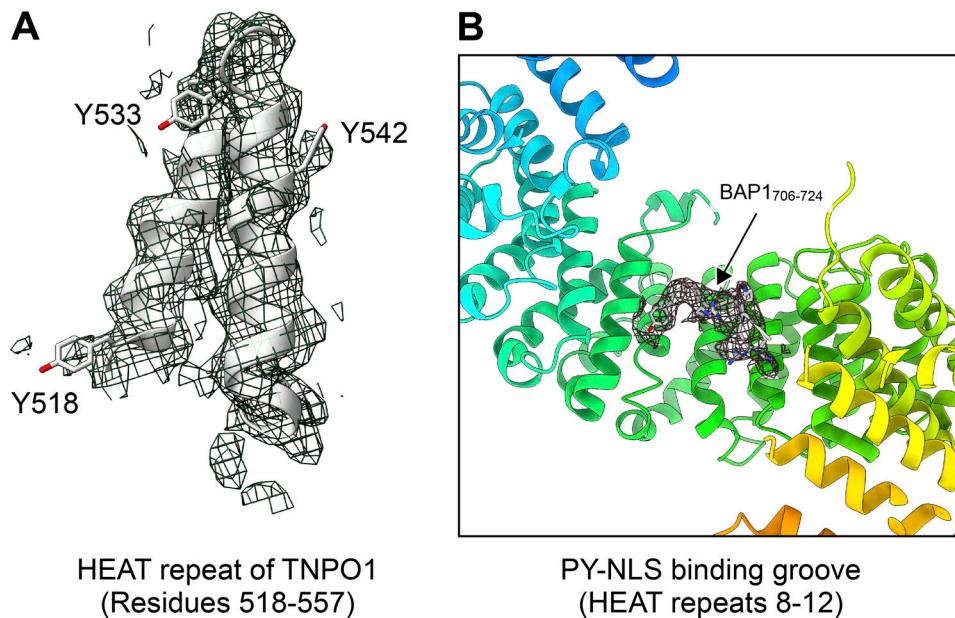
Figure S3. **Detailed view of the TNPO1:BAP1₇₀₆₋₇₂₄ complex with corresponding electron density. (A and B)** Cartoon and stick representation of a single HEAT repeat from the residues 518–557 of TNPO1 (A) and the BAP1₇₀₆₋₇₂₄ peptide (B) are shown with corresponding 2mFo-Fc composite omit maps contoured at 1σ. The corresponding 2mFo-Fc maps of the highlighted regions have limited the display to a zone within the range (r) of 3 Å of selected atoms by using the function "volume zone" in UCSF ChimeraX.
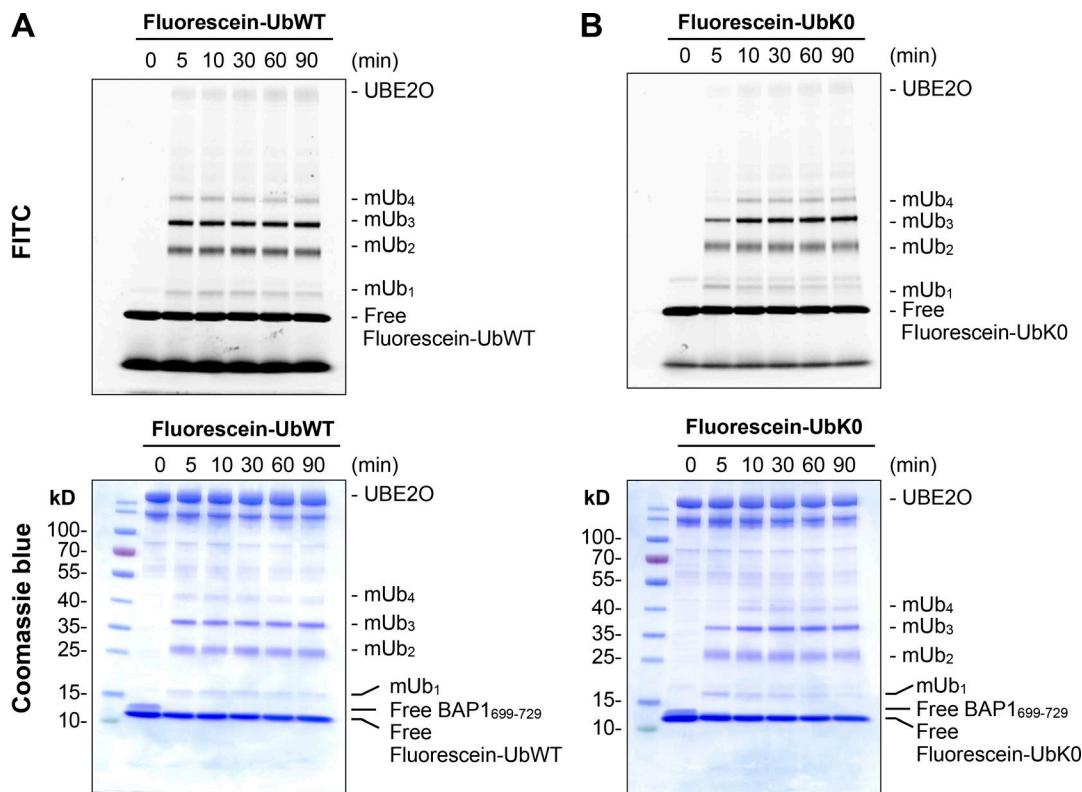
Figure S4. Establishment of UBE2O-dependent in vitro monoubiquitination using the unlabeled NLS peptide of BAP1 and different fluorescein-labeled ubiquitins. (A and B) In vitro monoubiquitination of $BAP1_{699-729}$ peptide treated with fluorescein-labeled WT ubiquitin (fluorescein-Ub_{WT}; A) or ubiquitin variant (fluorescein-Ub_{K0}, all lysine residues to alanine residues; B) detected by in-gel fluorescence with FITC channel and SDS-PAGE analyses with Coomassie blue staining. Source data are available for this figure: SourceData FS4.
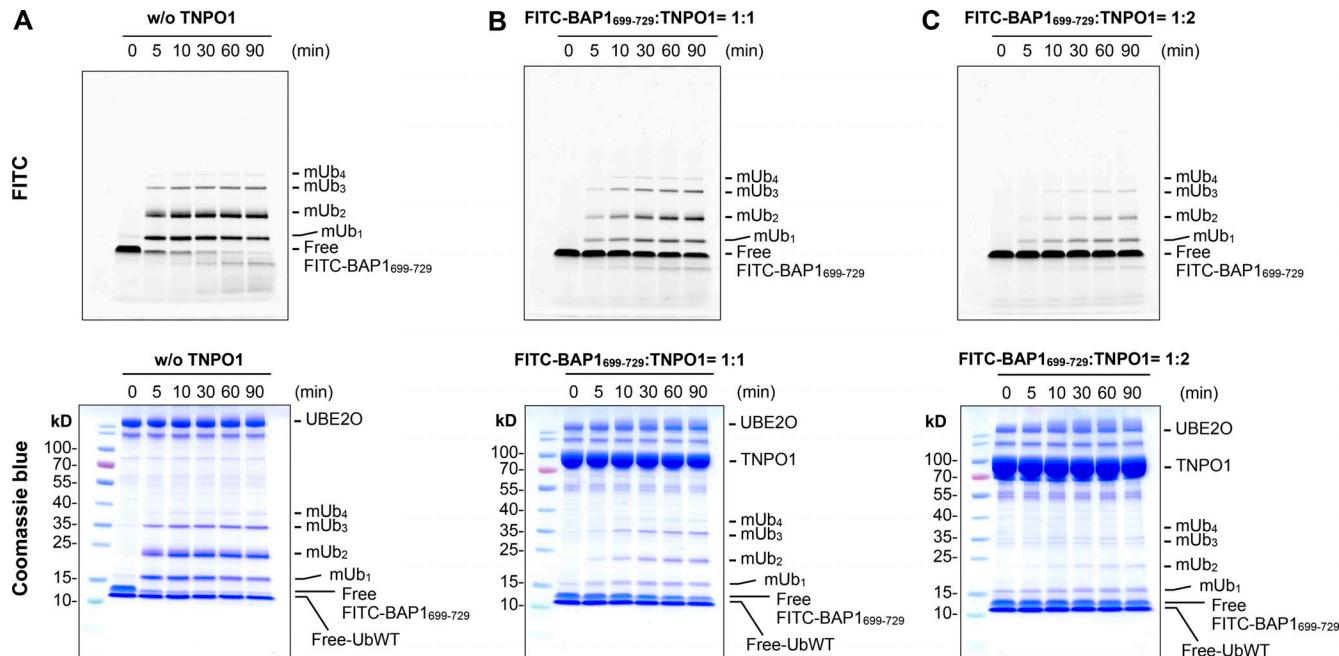

Figure S5. In vitro monoubiquitination of FITC-labeled $BAP1_{699-729}$ in the absence of TNPO1 and the presence of TNPO1 with different molar ratios. (A–C) Uncropped gel images corresponding to Fig. 6, D–F, with the detection contents of all protein materials used in the reaction by Coomassie blue staining. Source data are available for this figure: SourceData FS5.

Yang et al.
BAP1 nuclear import is governed by TNPO1

Journal of Cell Biology   S4
https://doi.org/10.1083/jcb.202201094

Provided online is Table S1. Table S1 lists the BAP1-associated proteins identified by AP-MS.

Yang et al.
BAP1 nuclear import is governed by TNPO1

Journal of Cell Biology   S5
https://doi.org/10.1083/jcb.202201094